Cellular and Molecular Life Sciences (2022) 79:249
https://doi.org/10.1007/s00018-022-04268-4

ORIGINAL ARTICLE

Traumatic-noise-induced hair cell death and hearing loss is mediated by activation of CaMKKβ

Fan Wu[1,2] · Kayla Hill[1] · Qiaojun Fang[1,3] · Zuhong He[1] · Hongwei Zheng[1] · Xianren Wang[1] · Hao Xiong[1] · Su-Hua Sha[1]

Received: 21 September 2021 / Revised: 14 March 2022 / Accepted: 20 March 2022 / Published online: 19 April 2022

Abstract

Background The Ca^{2+}/calmodulin-dependent protein kinase kinases (CaMKKs) are serine/threonine-directed protein kinases that are activated following increases in intracellular calcium, playing a critical role in neuronal signaling. Inner-ear-trauma-induced calcium overload in sensory hair cells has been well documented in the pathogenesis of traumatic noise-induced hair cell death and hearing loss, but there are no established pharmaceutical therapies available due to a lack of specific therapeutic targets. In this study, we investigated the activation of CaMKKβ in the inner ear after traumatic noise exposure and assessed the prevention of noise-induced hearing loss (NIHL) with RNA silencing.

Results Treatment with short hairpin RNA of CaMKKβ (shCaMKKβ) via adeno-associated virus transduction significantly knocked down CaMKKβ expression in the inner ear. Knockdown of CaMKKβ significantly attenuated noise-induced hair cell loss and hearing loss (NIHL). Additionally, pretreatment with naked CaMKKβ small interfering RNA (siCaMKKβ) attenuated noise-induced losses of inner hair cell synapses and OHCs and NIHL. Furthermore, traumatic noise exposure activates CaMKKβ in OHCs as demonstrated by immunolabeling for p-CaMKI. CaMKKβ mRNA assessed by fluorescence *in-situ* hybridization and immunolabeling for CaMKKβ in OHCs also increased after the exposure. Finally, pretreatment with siCaMKKβ diminished noise-induced activation of AMPKα in OHCs.

Conclusions These findings demonstrate that traumatic-noise-induced OHC loss and hearing loss occur primarily via activation of CaMKKβ. Targeting CaMKKβ is a key strategy for prevention of noise-induced hearing loss. Furthermore, our data suggest that noise-induced activation of AMPKα in OHCs occurs via the CaMKKβ pathway.

Keywords Adeno-associated virus-mediated gene silencing · Prevention of noise-induced hearing loss by RNA silencing *in-vivo* · Fluorescence *in-situ* hybridization in adult mouse cochleae · Activation of CaMKKβ after traumatic noise exposure

Abbreviations

AAV	Adeno-associated virus
ABR	Auditory brainstem response
AMPKα	AMP-dependent protein kinase α subunit
CaMKKβ	Ca^{2+}/calmodulin-dependent protein kinase kinase-β
DPOAE	Distortion product otoacoustic emissions
eGFP	Enhanced green fluorescent protein
FISH	Fluorescent *in-situ* hybridization
HCs	Hair cells
IHCs	Inner hair cells
IP	Intraperitoneal injection
KO	Knockout mice
LKB1	Liver kinase B1
MET	Mechanoelectrical transducer channels
NIHL	Noise-induced hearing loss
OHCs	Outer hair cells
PBS	Phosphate-buffered saline
PBS-T	PBS with 0.1% Tween 20
PTS	Permanent threshold shift

✉ Su-Hua Sha
shasu@musc.edu

[1] Department of Pathology and Laboratory Medicine, The Medical University of South Carolina, Walton Research Building, Room 403-E, 39 Sabin Street, Charleston, SC 29425, USA

[2] Department of Otolaryngology, Sun Yat-Sen Memorial Hospital, Sun Yat-Sen University, Guangzhou, China

[3] School of Life Sciences and Technology, Southeast University, Nanjing 210096, China

PTSN	PTS-noise
ROS	Reactive oxygen species
RWM	Round window membrane
SDS-PAGE	Sodium dodecyl sulfate polyacrylamide gel electrophoresis
SPL	Sound pressure level
siRNA	Small interfering RNA silencing
shRNA	Short hairpin RNA silencing
siControl	Scrambled siRNA
TTS	Temporary threshold shift
TDT	Tucker Davis Technology

Background

The World Health Organization reports that 5% of the world's population suffers from hearing loss and an estimated one in every ten people will have some degree of hearing loss by the year 2050. Acquired hearing loss accumulates over a lifetime, caused by insults like noise exposure. Corresponding to functional deficits, loss of sensory hair cells is the primary pathology of noise-induced hearing loss (NIHL). Since mammalian hair cells do not regenerate, such hearing loss is permanent. Considering the personal suffering and economic cost of hearing loss, its prevention has to be a high-priority health concern. However, no established pharmacological treatments for prevention or mitigation of NIHL exist. This is in part due to the complexity of sensory hair cell death pathways in response to the noxious challenges and the uncertainty of potential molecular targets. Also in question is the optimal delivery route of agents for prevention of hearing loss, since the inner ear has the blood–labyrinth barrier (BLB), which restricts entry of compounds into inner ear tissues [40].

Among the biochemical and pathological events identified in animal models, calcium (Ca^{2+}) has been implicated as a key factor in cell death signaling in a variety of cell types in response to a wide range of stimuli [44]. Ca^{2+} overload and disruption of intracellular Ca^{2+} homeostasis can trigger apoptotic or necrotic cell death through the activation of Ca^{2+}-dependent enzymes and signaling pathways. Calcium overload in sensory hair cells is well documented after traumatic noise exposure [17]. As the level of intracellular Ca^{2+} increases, calmodulin (CaM), a Ca^{2+}-binding protein, is expressed ubiquitously and acts as the primary intracellular Ca^{2+} receptor, binding free Ca^{2+} via its two Ca^{2+}-binding sites. This Ca^{2+}/CaM complex changes the conformation of CaM, allowing it to interact with a variety of proteins, including Ca^{2+}/CaM-dependent protein kinases (CaMKs), such as CaMKI, CaMKII, CaMKIV, and protein kinase kinases (CaMKKs). The binding of Ca^{2+}/CaM exposes an activating loop on CaMKI and CaMKIV that can be activated by CaMKKs. Therefore, p-CaMKI and p-CaMKIV serve as markers for activation of CaMKKs [18, 45, 50]. These kinases are involved in Ca^{2+}-dependent signaling cascades, regulating the activation of transcription factors [28, 37]. CaMKKs are composed of two isoforms, CaMKKα and CaMKKβ, CaMKKβ being expressed primarily in the brain and neuronal tissues and playing a critical role in neuronal signaling processes [54]. CaMKKβ also activates AMP-activated protein kinase (AMPK), a cellular energy sensor that regulates the energy balance of the cell [24]. AMPK is able to detect and react to the ATP level of the cell [67]. In response to energy depletion, the AMPK γ-subunit allosterically binds AMP, exposing the threonine 172 (T172) residue of the catalytic α-subunit. An activating phosphorylation on T172 occurs via upstream kinases, such as liver kinase B1 (LKB1). In contrast to that directed by AMP/LKB1, the CaMKKβ-dependent activation of AMPK is independent of AMP, instead requiring a change in intracellular calcium concentration [1]. Activation of AMPK directs the cell to switch off energy-consuming activities and switch on energy-generating pathways to help restore the energy balance of the cell [4, 19, 26, 67]. We have reported that traumatic noise transiently depletes cellular energy reserves and increases p-AMPKα T172 in outer hair cells (OHCs) in a noise-intensity-dependent manner [7, 22]. Furthermore, we found an association of AMPKα with reactive oxygen species (ROS) in OHCs after traumatic noise exposure [68].

Due to the BLB, systemic treatment with a compound might require high dosages to achieve therapeutic potential in the inner ear, increasing the risk of side effects. However, the inner ear is a relatively closed space surrounded by bone and separated from other systems. Substances applied to the perilymph have been shown to readily reach all the cells of the inner ear [59]. In recent years, several AAV vectors have been reported to infect sensory hair cells, and have been used to treat genetic hearing loss [2, 25, 32]. Furthermore, biopharmaceutical therapy using small interfering RNA (siRNA), short hairpin RNA (shRNA), and microRNA (miRNA) has emerged as next-generation medicine and RNAi-based therapeutic approaches have been successfully documented in other systems, for example, for diabetes, diabetic nephropathy, and diabetic retinopathy [6, 52]. In the inner ear, we have reported that local delivery of small interfering AMPKα RNA (siAMPKα) onto the round window membrane (RWM) attenuates noise-induced loss of inner hair cell (IHC) synapses and loss of OHCs, and prevents NIHL [22]. This protective effect is stronger than systemic treatment with compounds that we have tested, such as the antioxidant agent N-acetylcysteine (NAC), autophagy stimulator rapamycin, HDAC inhibitor SAHA, G9a inhibitor BIX-01294, and the mitochondrial calcium uniporter (MCU) inhibitor Ru360 [8, 64, 69, 73, 74].

In this study, we investigate the activation of CaMKKβ in the inner ear and its relationship to hair cell damage caused

by traumatic noise exposure in animal models. Mice are widely used in hearing research [42] and we have employed both CBA/J and FVB/NJ mice in this study. CBA mice are well characterized for NIHL due to their lack of the *Ahl* mutation in cadherin 23, which causes accelerated hearing loss. Unfortunately to our studies, CBA mothers will not continue to nurse and care for their pups when they are returned after handling and manipulation, regardless of how carefully we take care of the pups. In contrast, FVB/NJ mothers reliably accept their pups after experimental manipulations. Importantly, FVB/NJ mice show normal baseline hearing thresholds up to 10–12 weeks of age and display similar sensitivity to noise-induced loss of sensory hair cells as CBA/J mice [23]. We therefore used FVB/NJ mice for experiments on short hairpin RNA silencing (shRNA) via AAV2.7m8 virus transduction. We also employ cutting-edge technologies with fluorescent *in-situ* hybridization (FISH) with RNAscope and small interfering RNA silencing (siRNA) with adult CBA/J mice to address whether traumatic-noise-induced sensory hair cell death is mediated by activation of CaMKKβ. To our knowledge, our study is the first demonstrating that CaMKKβ can be safely silenced in the inner ear via AAV transduction, which provides significant insight for investigation of the mechanisms of NIHL.

Results

Short-hairpin-RNA-mediated CaMKKβ silencing via AAV2.7m8 transduction significantly silences CaMKKβ expression in sensory hair cells and the inner ear of FVB/NJ mice

To assess the role of CaMKKβ in traumatic-noise-induced hair cell loss and hearing loss, we first employed short-hairpin-RNA-mediated CaMKKβ silencing (shCaMKKβ) via virus transduction (AAV2.7m8). Since FVB/NJ mice show normal baseline hearing up to at least 10–12 weeks of age and show similar sensitivity to noise-induced loss of OHCs in basal turns as CBA/J mice, we used FVB/NJ mice in experiments with shCaMKKβ manipulation as FVB/NJ mothers take normal care of their AAV-injected pups. Based on a report that AAV2.7m8 infects cochlear IHCs and OHCs with high efficiency [25], we applied scrambled shRNA (shControl) or shCaMKKβ via AAV2.7m8 transduction by injection of virus vectors into the RWM of the left ears of postnatal 1–2 d (p1–2) pups. Three weeks after virus injections, the infection rate was 100% in IHCs along the entire cochlear spiral, 90% for OHCs in the basal and middle turns, and 40% for OHCs in the apical turn by counts of eGFP-positive sensory hair cells. There was no difference in the infection rates between shControl and shCaMKKβ in sensory hair cells (Fig. 1A–B). shCaMKKβ showed about 70% silencing efficiency of CaMKKβ compared with shControl mice measured by Western blots using whole cochlear homogenates 3 weeks after virus injections (Fig. 1C, F2, 15 = 67.28, $p < 0.001$). There was no difference in CaMKKβ expression between shControl and control mice without virus injection ($p > 0.05$). AAV transfection of shControl and shCaMKKβ to mice produced similar GFP band densities, confirming the lack of difference in transfection rates. Additionally, injection of virus vectors into p1–2 pups did not induce hearing loss as measured by ABRs and DPOAEs 3–4 weeks after injections. Auditory thresholds at all three tested frequencies (8, 16, and 32 kHz) and DPOAE amplitudes from 4 to 36 kHz were similar between control (naive control with no shRNA treatment), shControl, and shCaMKKβ groups (Fig. 2, A: ABR thresholds; 8 kHz: $F_{2, 21} = 0.687$, $p = 0.514$; 16 kHz: $F_{2, 21} = 1.108$, $p = 0.349$; 32 kHz: $F_{2, 21} = 0.061$, $p = 0.941$; B: DPOAE amplitude; $F_{2, 17} = 0.353$, $p = 0.707$), in agreement with the literature [25, 32]. These data indicate that AAV transduction effectively silences CaMKKβ and provides an excellent platform for studying gain and loss of function.

AAV2.7m8-mediated CaMKKβ silencing by shRNA significantly protects from traumatic noise-induced hair cell loss and hearing loss in FVB/NJ mice

Next, we characterized noise conditions by exposing 4-week-old FVB/NJ mice to noise intensities ranging from 96 to 100 dB SPL for 2 h as previously reported [23]. Auditory thresholds were measured before and 2 weeks after noise exposure. Threshold shifts were calculated as baseline thresholds subtracted from post-exposure thresholds of each individual mouse. Control mice without exposure had no shifts. Permanent threshold shifts (PTS) occurred in FVB/NJ mice after exposure to 100 dB SPL, showing shifts on average of 75 dB at 32 kHz, 60 dB at 16 kHz, and 35 dB at 8 kHz without differences between male and female mice (Fig. 3A). Such a pattern of hearing loss is similar to CBA/J mice [22, 73]. We then counted loss of OHCs along the entire cochlear spiral after the final ABR measurement. Loss of OHCs mainly appeared in the hook and basal turns, but no inner hair cell loss occurred (Fig. 3B). We, therefore, used this PTS condition for *in-vivo* experiments to assess if shCaMKKβ attenuates noise-induced loss of sensory hair cells and NIHL. Fourteen days after 100-dB noise exposure, loss of OHCs appeared in the hook and the basal turns with clearly greater loss of OHCs in the hook area. There was no OHC loss in the middle turn (Fig. 3B). Counts of OHC loss along the entire length of cochlear spiral showed noise-induced loss of OHCs in the basal turn starting at 3.75 mm from the apex with a gradient of increased loss toward the hook region until 65% OHC loss was reached at 5.5 mm (Fig. 4A). In shControl mice, noise-induced loss of OHCs

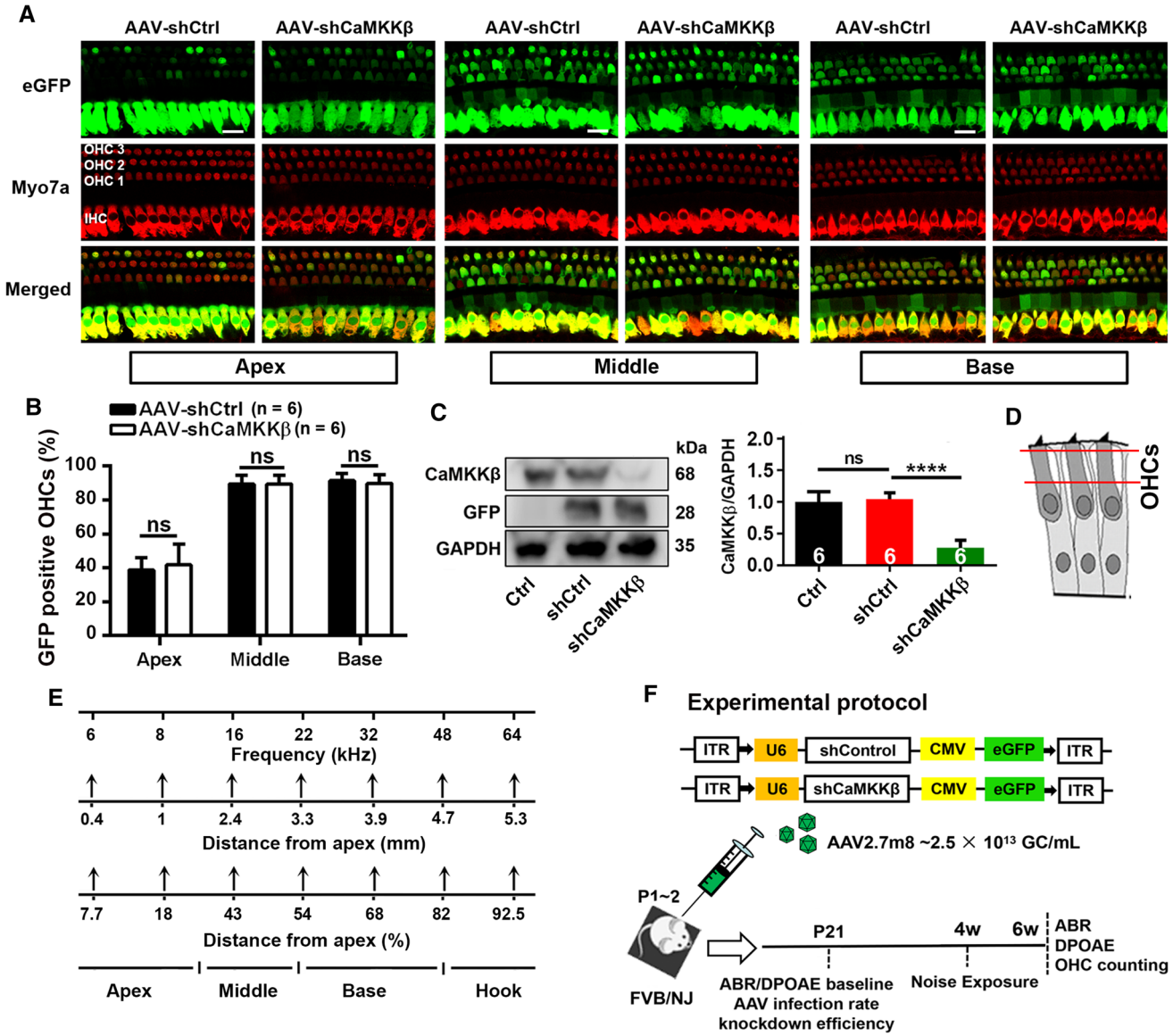

Fig. 1 Application of shCaMKKβ via adeno-associated virus transduction significantly reduces CaMKKβ expression in the inner ear of FVB/NJ mice. **A** Representative images show AAV-infected sensory hair cell expression of eGFP (green) in the apical, middle, and basal turns co-localized by immunolabeling for myosin VIIa (Myo7a, red). Cochleae were harvested at p21 after microinjection of 2 µL of AAV-shControl (shCtrl) or AAV-shCaMKKβ stock solutions (2.5×10^{13} GC/mL) into the left ear of FVB/NJ mice at p1–2. eGFP: enhanced green fluorescent protein, Myo7a: myosin VIIa antibody used as a specific marker for sensory hair cells, shCtrl: scrambled shRNA, AAV-shCtrl: AAV2.7m8-U6-shControl-CMV-eGFP, and AAV-shCaMKKβ: AAV2.7m8-U6-shCaMKKβ-CMV-eGFP. Scale bar = 10 µm. **B** Counts of the eGFP-positive sensory hair cells show there was no difference in the infection rates between shCtrl and shCaMKKβ in OHCs and inner hair cells (IHCs) with an infection rate in IHCs of nearly 100% and 90% in OHCs in the middle and basal turns and 40% in OHCs in the apical turn. Data are presented as means + SD, $n = 6$ in each group, *ns* not statistically significant. **C** Representative images of immunoblots using inner ear homogenates revealed the bands of CaMKKβ, GFP, and GAPDH. GFP served as the transfection marker and GAPDH as the sample loading control. Quantification of the CaMKKβ band density shows significant reduction by 70% in shCaMKKβ via virus transduction compared with shCtrl mice. Data are presented as means + SD, $n = 6$ in each group, $^{****}p < 0.0001$. **D** The schematic diagram of OHCs indicates the plane from which confocal immunofluorescence images were captured, the cytosolic area between the two red lines. OHCs indicate outer hair cells. **E** A schematic diagram indicates mapping of frequencies along the entire cochlear spiral. **F** This diagram illustrates the AAV vector plasmid and the experimental timeline in FVB/NJ mice

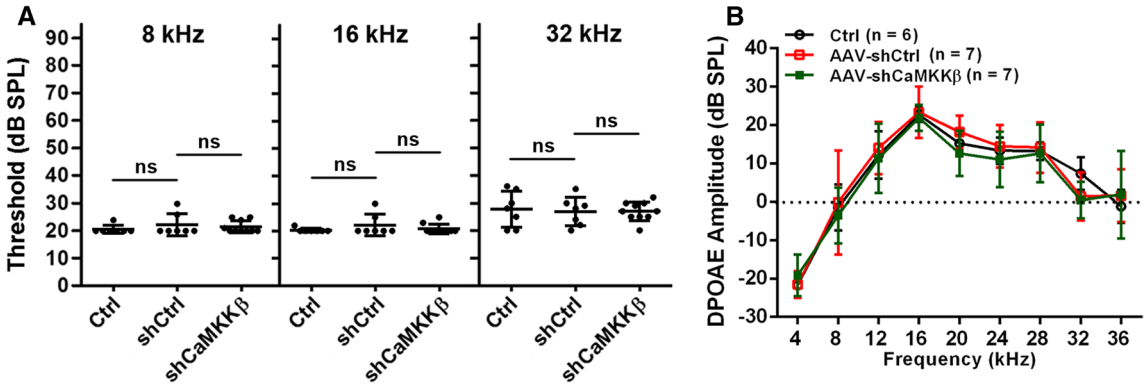

Fig. 2 Injection of AAV-shCtrl and AAV-shCaMKKβ to p1–2 FVB/NJ mice does not influence hearing and outer hair cell function. **A** Auditory baseline thresholds show no significant difference among the three groups (control mice without injection and AAV-shCtrl- and AAV-shCaMKKβ-injected mice) at all tested frequencies (8, 16, and 32 kHz) measured after mice were weaned at postnatal day 21. Data are presented as individual points with means ± SD, ns: not significant. **B** DPOAE amplitudes show similar waveforms from 4 to 36 kHz among the above three groups. Data are presented as means ± SD, $n = 6–7$ in each group

occurred in a similar pattern as non-virus-transduced mice (from 3.75 to 5.5 mm: $F_{1,\ 11} = 0.232$, $p = 0.639$), implying that AAV2.7m8 infection alone has no effect on the sensitivity of FVB/NJ mice to noise-induced OHC loss. In contrast, in shCaMKKβ silenced mice, noise-induced loss of OHCs was significantly decreased in the basal and hook regions (3.75–5.5 mm: $F_{1,13} = 148.532$, $p < 0.001$, Fig. 4A, for detailed statistical values see Table S1). In the hook area (5.0–5.5 mm from the apex), the percentage of noise-induced OHC loss was reduced from an average of 50% to less than 10% (Fig. 4A) as illustrated by representative images (Fig. 4B). Moreover, shCaMKKβ mice showed significant prevention of PTS-noise-induced auditory threshold shifts at all tested three frequencies (Fig. 4C, AAV-shCtrl + 100 dB vs AAV-shCaMKKβ + 100 dB: 8 kHz: $F_{2,\ 21} = 8.895$, $p < 0.01$; 16 kHz: $F_{2,\ 21} = 25.26$, $p < 0.0001$, 32 kHz: $F_{2,\ 21} = 24.64$, $p < 0.0001$). Auditory threshold shifts induced by PTS-noise exposure were similar at all three measured frequencies (8, 16, and 32 kHz) between AAV-shControl mice and control mice without AAV transduction 14 d after the exposure. Additionally, OHC functional testing by DPOAE measurements showed that the amplitudes peaked at 16 kHz in control mice without the exposure, whereas 14 d after the exposure, the peak disappeared and the wave flattened with an amplitude below -10 dB SPL at all tested frequencies from 4 to 36 kHz (Fig. 4D, Ctrl vs Ctrl + 100 dB, $F_{1,13} = 211.077$, $p < 0.001$). shControl mice showed similar DPOAE amplitudes after 100-dB noise exposure as the mice without virus transfection (Fig. 4D, $F_{1,12} = 0.099$, $p = 0.759$), while shCaMKKβ-silenced mice showed significant reversal of noise-diminished DPOAE amplitudes from 8 to 36 kHz with an amplitude peak at 16 kHz, although lower than control mice without exposure (Fig. 4D, AAV-shCtrl + 100 dB vs AAV-shCaMKKβ + 100 dB, $F_{1,13} = 56.405$, $p < 0.001$; for detailed statistical values see Table S2). All these results indicate that CaMKKβ silencing via AAV vectors has a significant preventive effect against NIHL in FVB/NJ mice.

Pretreatment with CaMKKβ small interfering RNA attenuates traumatic-noise-induced loss of outer hair cells and NIHL in CBA/J mice

We have characterized noise-induced hair cell loss and NIHL well in CBA/J mice [22, 73]. To test whether silencing CaMKKβ also attenuates NIHL in CBA/J mice at the age of 12 weeks, we applied scrambled-siRNA (siControl) or siCaMKKβ onto the RWM of mice 72 h before noise exposure, based on our previously established method [43]. The silencing efficiency in OHCs of siCaMKKβ-treated mice was about 40% reduction of CaMKKβ with delivery of 0.6 µg siCaMKKβ compared to that of siControls (Fig. 5A, B, $t_5 = 5.1711$, $p = 0.0036$). The selection of 0.6 µg siCaMKKβ for our experiments was based on our preliminary results. To induce PTS with losses of IHC synapses and OHCs without loss of IHCs, CBA/J mice were exposed to 101 dB for 2 h, referred to as PTSN. Pretreatment with siCaMKKβ significantly reduced noise-induced auditory threshold shifts at 8 ($F_{2,\ 37} = 4.106$, $p = 0.0245$), 16 ($F_{2,\ 37} = 69.55$, $p < 0.0001$) and 32 kHz ($F_{2,\ 37} = 28.11$, $p < 0.0001$) compared to that of siControl-treated mice 14 d after the exposure (Fig. 5C). Additionally, noise-induced auditory threshold shifts were similar between siCtrl and sham surgery groups (Fig. 5C). Furthermore, noise exposure significantly diminished DPOAE amplitudes from 8 to 36 kHz ($F_{1,\ 9} = 111.894$, $p < 0.001$) and this reduction was significantly alleviated with siCaMKKβ treatment (Fig. 5D $F_{1,\ 9} = 58.829$, $p < 0.001$; for detailed statistical values, see Table S3).

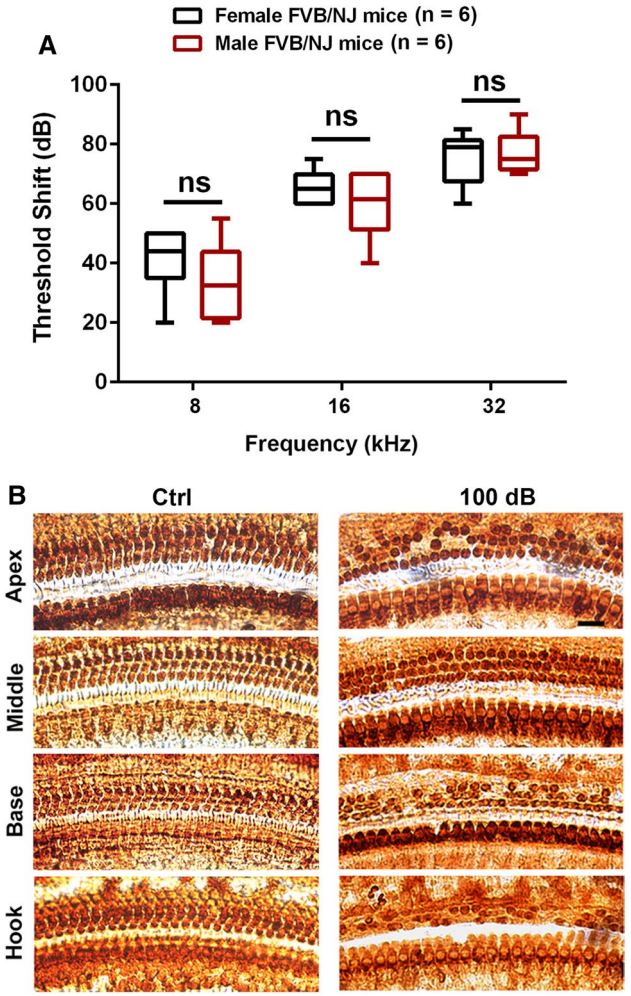

Fig. 3 Noise-induced hearing loss is similar between male and female FVB/NJ mice exposed at the age of 4 weeks. **A** Auditory threshold shifts were calculated as baseline thresholds (before exposure) subtracted from thresholds 14 d post-exposure for each individual mouse. Noise exposure at 100 dB for 2 h induces hearing loss at all three measured frequencies (8, 16, and 32 kHz) that is more severe at higher frequencies than lower frequencies in both male and female mice. Data are presented as means with minimum-to-maximum ranges, ns indicates no statistical difference between males and females. **B** Representative microscope images were taken from the apical, middle, basal, and hook turns of whole mount surface preparations immunolabeled with myosin VIIa and then stained with DAB to illustrate OHCs and IHCs. OHC 1, 2, 3, and IHC indicate three rows of outer hair cells and one row of inner hair cells. Counts of OHC loss are shown in Fig. 4A. These images are representative of six mice for each group. Scale bar = 10 µm

Likewise, pretreatment with siCaMKKβ significantly reduced noise-induced loss of OHCs by counts of OHCs along the entire length of the cochlear spiral with myosin-VIIa-labeled and DAB-stained whole-mount surface preparations (Fig. 5E, $F_{1,11} = 9.213$, $p = 0.011$; for detailed statistical values of Fig. 5F, see Table S4). In siControl-treated mice, noise-induced OHC loss started at 3.0 mm from the apex with a gradient of increased loss toward the base until complete OHC loss was reached 5.5 mm from the apex, while in siCaMKKβ-treated mice, noise-induced loss of OHCs began 4 mm from the apex and decreased to an average of 60% at 5.5 mm with significant decreases in OHC loss at 3.5 mm ($p = 0.044$), 4 mm ($p < 0.001$), and 4.5 mm ($p = 0.001$) from the apex. These results indicate that pretreatment with siCaMKKβ attenuates traumatic-noise-induced hair cell loss and NIHL in CBA/J mice, in line with results from knockdown of shCaMKKβ against traumatic-noise-induced hair cell loss and NIHL in FVB/NJ mice.

Pretreatment with CaMKKβ small interfering RNA protects against traumatic-noise-induced loss of inner hair cell synaptic ribbons in CBA/J mice

Noise-induced loss of IHC synapses has been well documented. Ribeye is a component of the ribbon. CtBP2 and ribeye share an epitope that is recognized by the anti-CeBP2 antibody. IHC synapses can be assessed by co-immunolabeling for CtBP2 for the presynaptic ribbon and Glu2A for the post-synaptic terminal [14, 22, 62]. We assessed whether pretreatment with siCaMKKβ can also prevent noise-induced loss of IHC synapses 14 d after the noise exposure. Previously, we found that treatment with siControl alone without noise exposure did not change the number of IHC synapses compared to the naive group (control) [22]. In siControl-treated mice, noise-induced loss of IHC synapses occurred at 22 and 32 kHz 14 d after exposure without the appearance of a significant amount of orphan ribbons (marked by separation of CtBP2 from GluA2 labeling) (Fig. 6A). Counts of synapses per IHC in the regions of 0.4, 1.0, 2.4, 3.3, and 3.9 mm from the apex (corresponding to 6, 8, 16, 22, and 32 kHz) after the noise exposure showed significant losses of IHC synapses at 22 ($F_{2,17} = 29.04$, $p < 0.0001$), and 32 kHz ($F_{2,15} = 22.83$, $p < 0.0001$) but not at 6, 8, and 16 kHz compared to siControl mice without exposure (Fig. 6B), while pretreatment with siCaMKKβ significantly reduced noise-induced loss of synapses in both the 22-kHz and 32-kHz regions ($p < 0.0001$), with the number of IHC synapses in siCaMKKβ-treated mice being similar to control mice without noise exposure (Fig. 6B). These results are in agreement with the protection of noise-induced hair cell loss and NIHL by pretreatment with siCaMKKβ.

Traumatic noise exposure reveals p-CaMKI-positive immunolabeled outer hair cells in both CBA/J and FVB/NJ mice

Since CaMKKβ is one of the kinases upstream of AMPKα, our previous report showed that noise activates p-AMPKα T172 and silencing AMPKα prevents NIHL [22], we also assessed the activation of CaMKKβ in CBA/J mice.

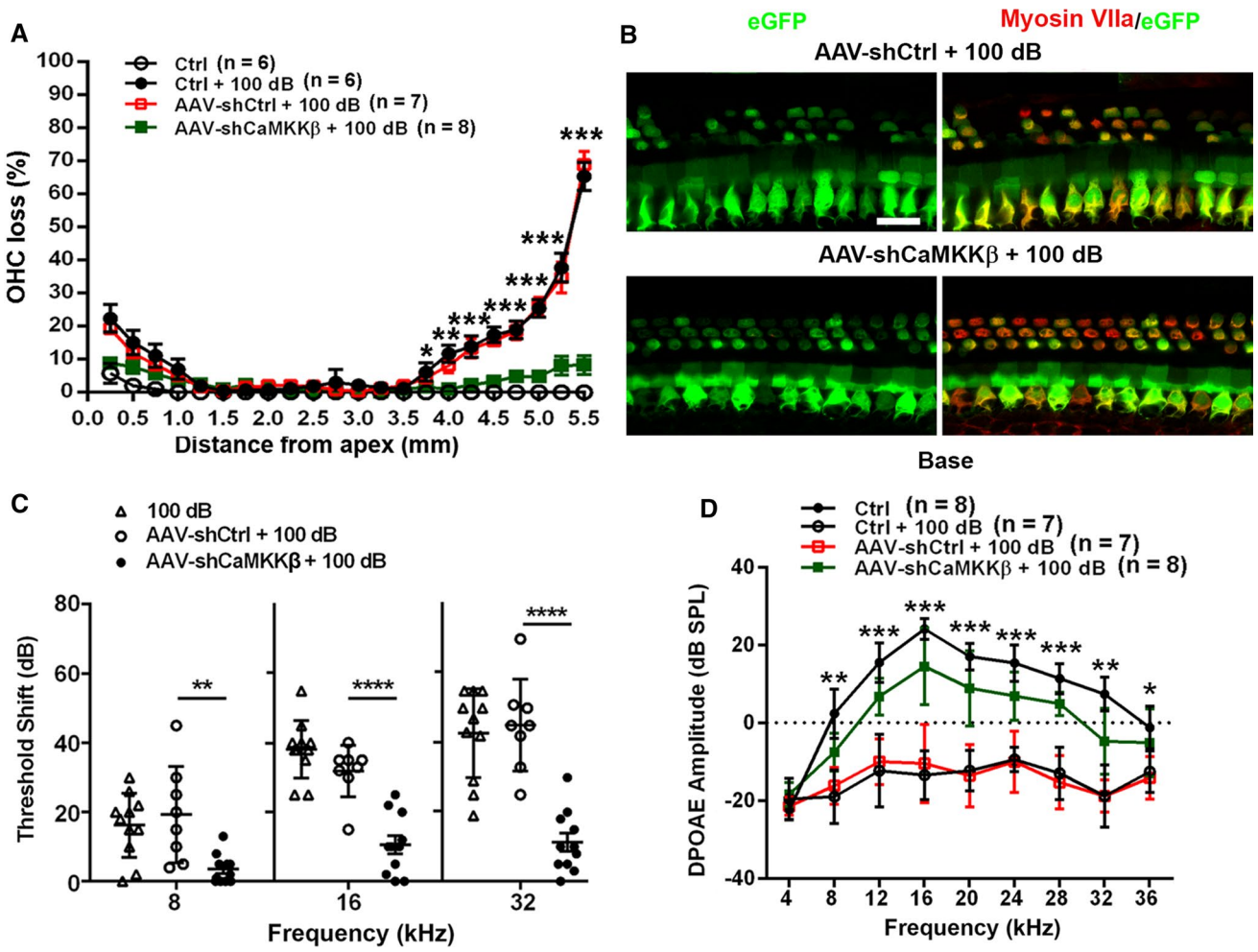

Fig. 4 Application of shCaMKKβ via adeno-associated virus transduction significantly protects against noise-induced loss of OHCs and NIHL in FVB/NJ mice. **A** Application of shCaMKKβ via AAV2.7m8 significantly reduces noise-induced OHC loss. Loss of OHCs was counted along the entire length of the cochlear spiral. Data are presented as means ± SE. The detailed statistical values are listed in Table S1. **B** Surface preparations show that AAV-shCtrl or AAV-shCaMKKβ mice were immunolabeled with myosin VIIa (red) processed 14 d after the exposure. Images were taken from the lower basal cochlear turn. Scale bar = 20 µm. **C** Noise-induced auditory threshold shifts are significantly reduced in AAV-shCaMKKβ mice compared to AAV-shCtrl mice calculated as baseline ABR thresholds subtracted from thresholds measured 14 d after noise exposure for each individual mouse. Data are presented as individual mice ± SD. **D** Noise-diminished DPOAE amplitudes are significantly reversed by shCaMKKβ application measured 14 d after noise exposure. Data are presented as means ± SD. The detailed statistical values are listed in Table S2; *indicates the *p* value of the comparison between shCtrl + noise exposure vs shCaMKKβ + noise exposure, $*p < 0.05$, $**p < 0.01$, $***p < 0.001$, $****p < 0.0001$

Phosphorylated CaMKI (p-CaMKI T177) serves as one of the markers for CaMKKβ activation [18, 45], and thus, we assessed p-CaMKI (T177) in OHCs by immunohistochemistry after traumatic noise exposure at several time points. We found that immunolabeling for p-CaMKI appeared in the stereocilia and cuticular plates of structurally damaged OHCs, but not in intact OHCs or scars of lost OHCs (Fig. 7A, A' enlarged OHCs in the right panel), when examined 1, 3, 5, and 8 h after the traumatic noise exposure and decreased with time post-exposure until no p-CaMKI-positive OHCs were seen 24 h after the exposure. P-CaMKI-positive OHCs appeared only in the hook and basal turns (4.5–5.5 mm from apex) of the cochlear epithelia at the examined time points. Counts of p-CaMKI-positive OHCs 1–3 h after completion of noise exposure showed positive labeling in an average of 18% of OHCs in the regions between 4.5 and 5.5 mm from the apex (hook and lower basal turns) (Fig. 7B, $t_{10} = 5.791$, $p = 0.0002$). Similar immunolabeling for p-CaMKI in OHCs after traumatic noise exposure appeared also in FVB/NJ mice. Additionally, to determine the specificity of antibodies used for immunohistochemistry, we employed Western blots using mouse whole cochlear tissue homogenates. A single protein band for p-CaMKI at the correct molecular weight of 45 kDa was confirmed (Fig. 7C). Semi-quantification

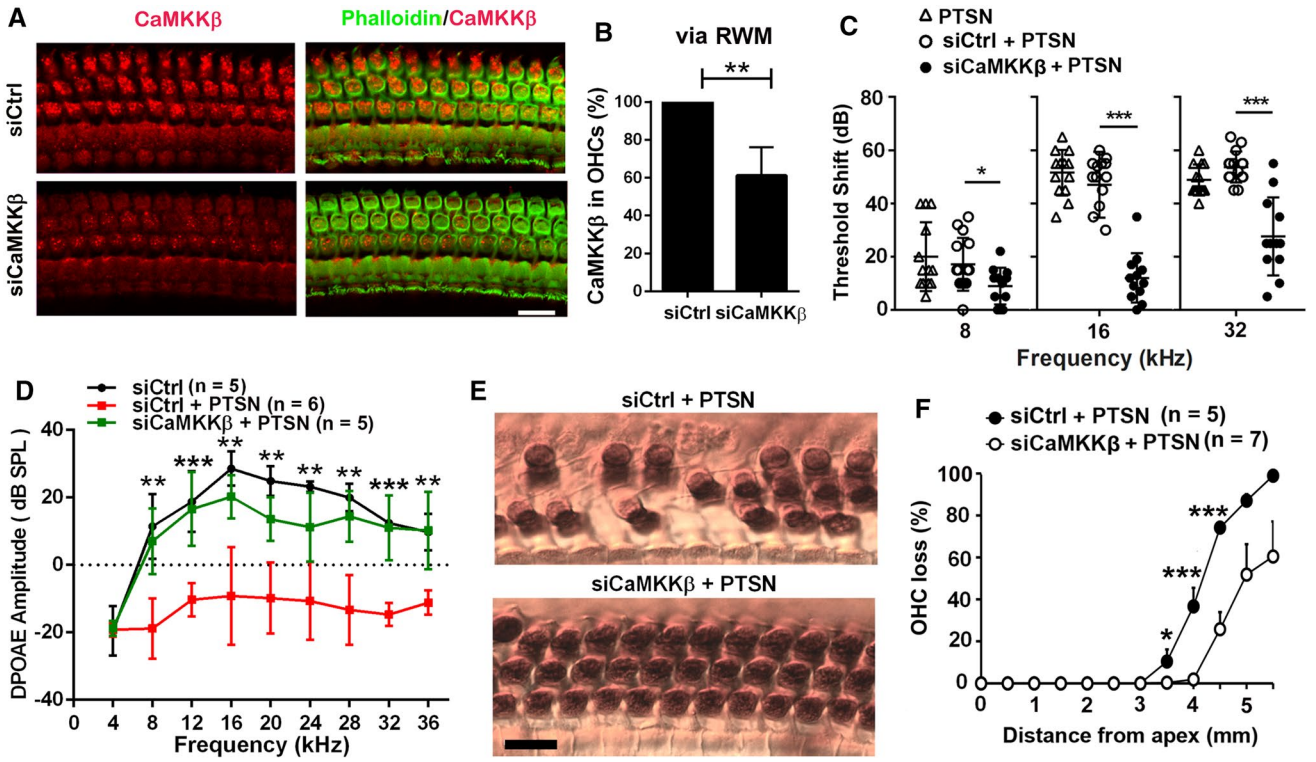

Fig. 5 Pretreatment with CaMKKβ siRNA via intra-tympanic delivery reduces noise-induced loss of OHCs and NIHL in CBA/J mice. **A** Representative images exhibit reduction of CaMKKβ-associated immunoreactivity (red) in OHCs 72 h after intra-tympanic delivery of siCaMKKβ to the left ears of mice compared to those of siControl mice. Red: immunolabeling for CaMKKβ; green: phalloidin fluorescence for localization of OHCs. Scale bar = 10 µm. **B** Semi-quantification of CaMKKβ immunolabeling in OHCs of the basal turn via RWM delivery confirms a significant decrease with siCaMKKβ treatment (40%) compared to siControl. Data are presented as means + SD, $n = 5$. **C** Pretreatment with siCaMKKβ significantly decreases noise-induced auditory threshold shifts at 16 and 32 kHz. Data are presented as individual points and means ± SD. **D** Pretreatment with siCaMKKβ significantly attenuates PTS-noise-diminished DPOAE amplitudes from 8–36 kHz. Data are presented as means ± SD. Detailed statistical values are listed in Table S3. **E** Representative images reveal myosin-VIIa-labeled and DAB-stained OHCs (brown) 14 d after PTS-noise exposure (PTSN) in groups pretreated with siControl or siCaMKKβ. Images were taken from the basal turn at 4 mm from the apex and are representative of 5–7 mice for each group. Scale bar = 10 µm. **F** Counts of OHC loss along the entire length of the cochlear duct show that pretreatment with siCaMKKβ significantly reduced noise-induced OHC loss. Data are presented as means + SD. Detailed statistical values are listed in Table S4. The number of animals in each group is indicated in the labels, *indicates the p value for the comparison between siCtrl + PTSN vs siCaMKKβ + PTSN. *$p < 0.05$, **$p < 0.01$, ***$p < 0.001$

of p-CaMKI band densities showed no difference between control and traumatic-noise-exposed mice examined 1–3 h after the exposure or sham exposure (Fig. 7D p-CaMKI: $t_4 = 0.063$, $p = 0.953$). These results suggest that traumatic noise exposure activates CaMKKβ in OHCs.

Traumatic noise exposure increases CaMKKβ immunolabeling and CaMKKβ mRNA in outer hair cells of CBA/J mice

Next, we immunolabeled CaMKKβ in OHCs on whole-mount surface preparations 1–3 h and 24 h after completion of the exposure and found that the immunolabeling for CaMKKβ in OHCs in the basal turn was strong 24 h after the exposure (Fig. 8A), but only weakly increased at the 1–3 h time point. Semi-quantification of grayscale intensities of CaMKKβ in the OHCs in the basal turn confirmed a significant increase to twice that of controls 24 h after exposure ($t_5 = 3.098$, $p = 0.0269$), but no significant difference 1–3 h after (Fig. 8B). Additionally, immunoblots using mouse whole cochlear tissue homogenates also showed no difference between control and exposed mice, but a single protein band for CaMKKβ at the correct molecular weight of 68 kDa was confirmed (Fig. 8C, D, CaMKKβ: $t_4 = 0.959$, $p = 0.392$).

To determine if traumatic noise exposure changes CaMKKβ mRNA levels, we utilized FISH with RNAscope on cochlear surface preparations as described in prior reports [27, 49]. In general, the expression of CaMKKβ mRNA levels in sensory hair cells was low in control mice without exposure. Since loss of OHCs occurred in the hook and lower basal turn in a base-to-apex gradient 1 and 24 h after the completion of the exposure, it was impossible to quantify OHC CaMKKβ

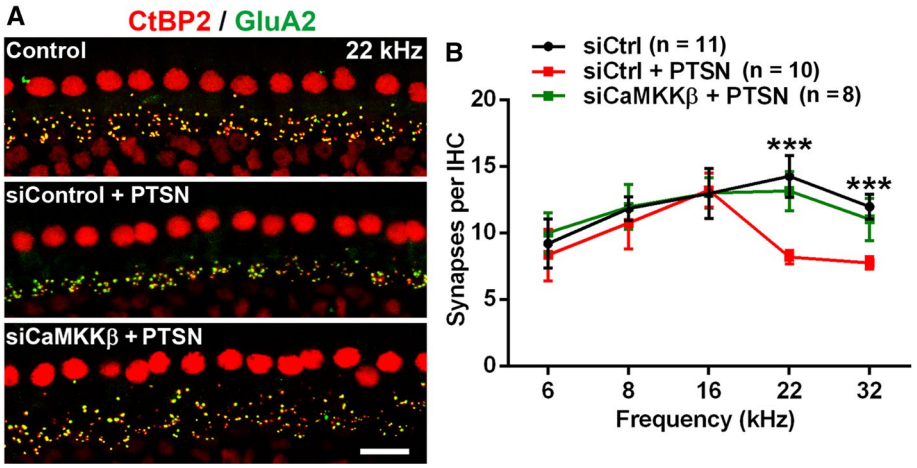

Fig. 6 Pretreatment with CaMKKβ siRNA via intra-tympanic delivery reduces noise-induced loss of IHC synapses in CBA/J mice. **A** Representative images reveal immunolabeling for CtBP2 (red) and GluA2 (green) in the 22-kHz region of cochlear epithelia assessed 14 d after PTSN exposure. Images are compressed from 30 Z-stack projections. Scale bar = 10 µm. **B** Quantification of CtBP2/GluA2-immunolabeled synapse particles in IHCs corresponding to 6, 8, 16, 22, and 32 kHz shows significant reduction at 22 and 32 kHz by PTSN, while pretreatment with siCaMKKβ prevented noise-induced loss of IHC synapses. Data are presented as means + SE. The number of animals in each group is indicated in the labels; *indicates the p value for the comparison between siCtrl + PTSN vs siCaMKKβ + PTSN, ***$p < 0.001$

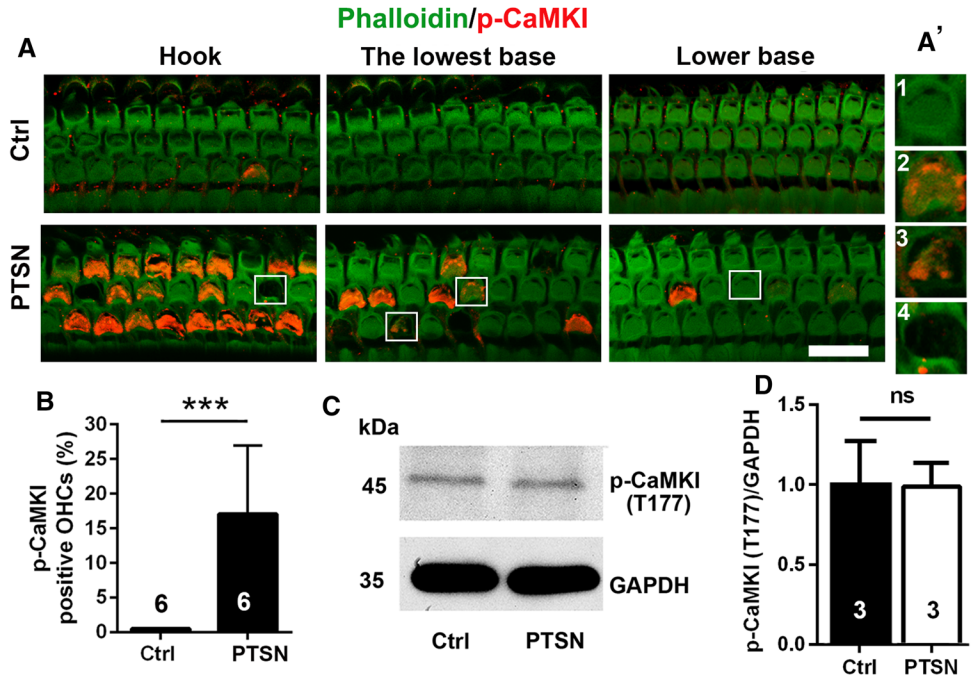

Fig. 7 Traumatic noise exposure activates CaMKI in OHCs of the basal turn of CBA/J mice. **A** OHCs of the basal region display immunolabeling for p-CaMKI (T177, red) in the cuticular plate of structurally damaged OHCs when processed 1–3 h after completion of traumatic noise exposure compared to control mice without the exposure. The representative images show the hook and lower basal turn and are representative of 6 mice each. PTSN: permanent threshold shift noise exposure; scale bar = 10 µm. **A'** the enlarged four OHCs show immunolabeling for p-CaMKI (Th177) in structurally damaged OHCs (2, 3), but not in intact OHCs (1) or scars of lost OHCs (4). **B** Counts of the number of OHCs displaying p-CaMKI (Thr177) immunolabeling in the hook and lower basal turns of the cochlear duct confirms a significant increase 1–3 h after completion of PTSN. Data are presented as means + SD. The number of animals in each group is indicated in the bar graph. ***$p < 0.001$. **C** Western blots using whole cochlear tissue homogenates reveal specificity for CaMKKβ and p-CaMKI (T177) but show no change in band densities for p-CaMKI (T177) examined 1–3 h after the noise exposure compared with unexposed controls. GAPDH serves as the loading control. The molecular weights are indicated to the right of the bands. Data are presented as means + SD. The number of animals in each group is indicated in the bar graphs, ns: not significant

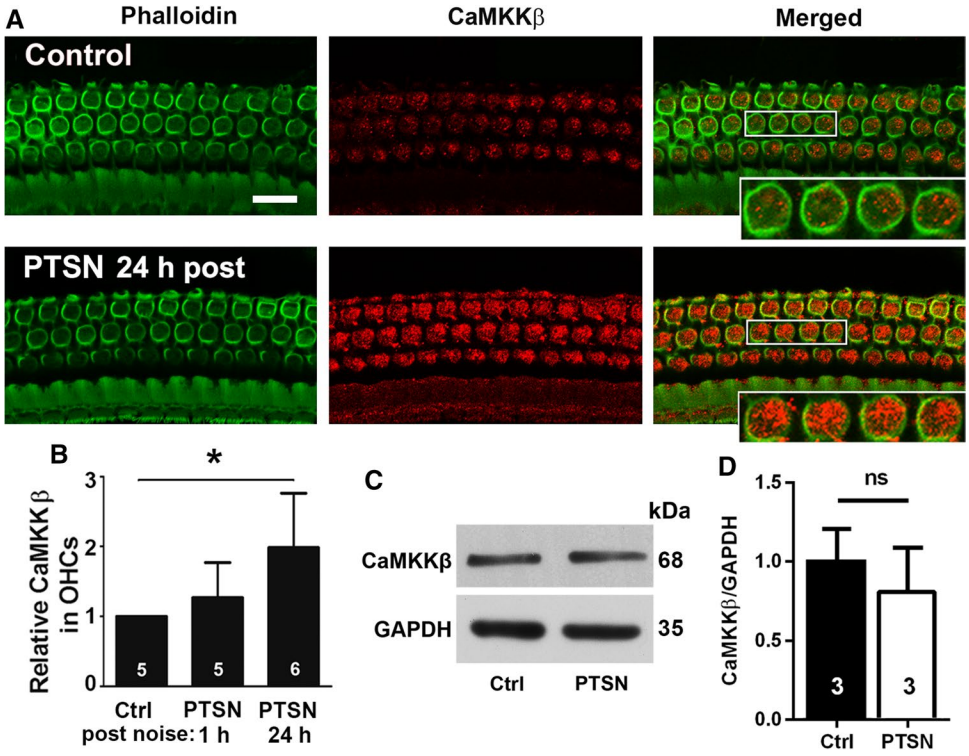

Fig. 8 Traumatic noise exposure increases immunolabeling for CaMKKβ in OHCs of CBA/J mice. **A** Immunolabeling for CaMKKβ (red) in OHCs of the basal turn appears stronger when processed 24 h after completion of the PTSN exposure (PTSN 24 h post) compared with unexposed controls. The enlarged OHCs allow for better visualization of punctate labeling for CaMKKβ; green: phalloidin-stained OHCs. Scale bar = 10 µm. **B** Semi-quantitative analysis of relative CaMKKβ labeling (grayscale) in OHCs confirms a significant increase when examined at 24 h, but not at 1–3 h after PTSN. Data are presented as means + SD; the number of animals in each group is indicated in the bar graph, $*p < 0.05$. **C** Immunoblots using whole cochlear tissue homogenates reveal specificity for CaMKKβ but show no change in band densities for CaMKKβ examined 1–3 h after the noise exposure compared with unexposed controls. GAPDH serves as the loading control. The molecular weights are indicated to the right of the bands. **D** Quantification of the band densities confirmed no difference between the two groups. The number of animals in each group is indicated in the bar graph, *ns* not significant

mRNA levels in the hook and lower basal turn. We, therefore, analyzed CaMKKβ mRNA in OHCs in the apical, middle, and basal turns at 1–3 h or 24 h after completion of the noise exposure (Fig. 9A). We found that puncta of CaMKKβ mRNA labeling are more prominent at 24 h than 1–3 h in preliminary experiments. We then focused on comparing control mice without exposure to traumatic-noise-exposed mice 24 h after the exposure. The expression of CaMKKβ mRNA levels in OHCs in the apical ($t_6 = 3.528$, $p = 0.0124$), middle ($t_5 = 3.4612$, $p = 0.018$), and basal turns ($t_6 = 5.247$, $p = 0.0019$) increased significantly by about twofold compared to that of control mice without noise exposure (Fig. 9B). These results suggest that the increased CaMKKβ mRNA and protein levels in OHCs 24 h after the exposure may signify a cellular feedback response.

Inhibition of CaMKKβ reduces the activation of AMPKα by noise in outer hair cells of CBA/J mice

To assess whether inhibition of CaMKKβ diminishes the activation of AMPKα in the inner ear, we pretreated mice with siCaMKKβ via delivery onto the RWM per our prior report [43]. In agreement with our previous publication [22, 68], traumatic noise exposure resulted in a significant increase in p-AMPKα in OHCs (Fig. 10A, B, $t_7 = 5.095$, $p = 0.0014$). Such increased immunolabeling for p-AMPKα (T172) in OHCs was reduced by pretreatment with siCaMKKβ (Fig. 10C). Semi-quantitative analysis of the grayscales of immunolabeled p-AMPKα (T172) confirmed a 25% reduction in OHCs (Fig. 10D, $t_4 = 5.024$, $p = 0.0074$). These results support the notion that CaMKKβ is one of the

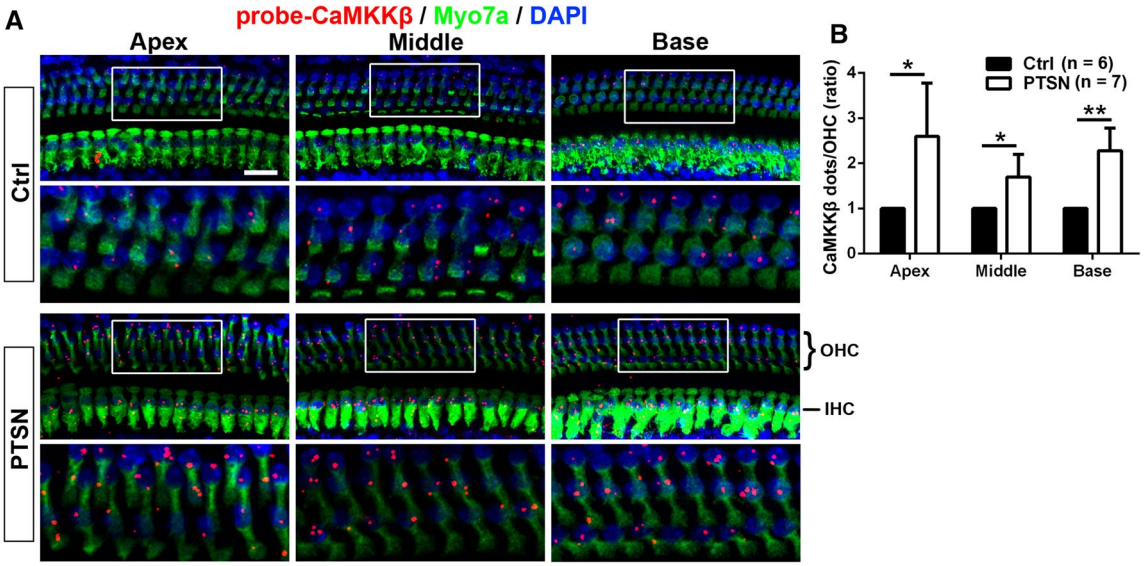

Fig. 9 Traumatic noise exposure increases CaMKKβ mRNA levels in OHCs of CBA/J mice. **A** Representative images illustrate FISH with RNAscope probed with CaMKKβ (red dots), immunolabeled with myosin-VIIa (Myo7a, green), and stained with DAPI (blue) of the apex, middle, and basal turns of mice exposed to PTSN examined 24 h after the exposure compared with unexposed controls (Ctrl). The lower panels are OHCs enlarged from the white rectangles in the upper panels for better visualization. Images are compressed from 30 Z-stack projections. OHCs: outer hair cells, IHC: inner hair cells. Scale bar = 10 μm. **B** Counts of red dots indicating CaMKKβ mRNA show a doubling 24 h after PTSN exposure. Data are presented as means + SD. The number of animals in each group is indicated in the labels, $*p < 0.05$, $**p < 0.01$

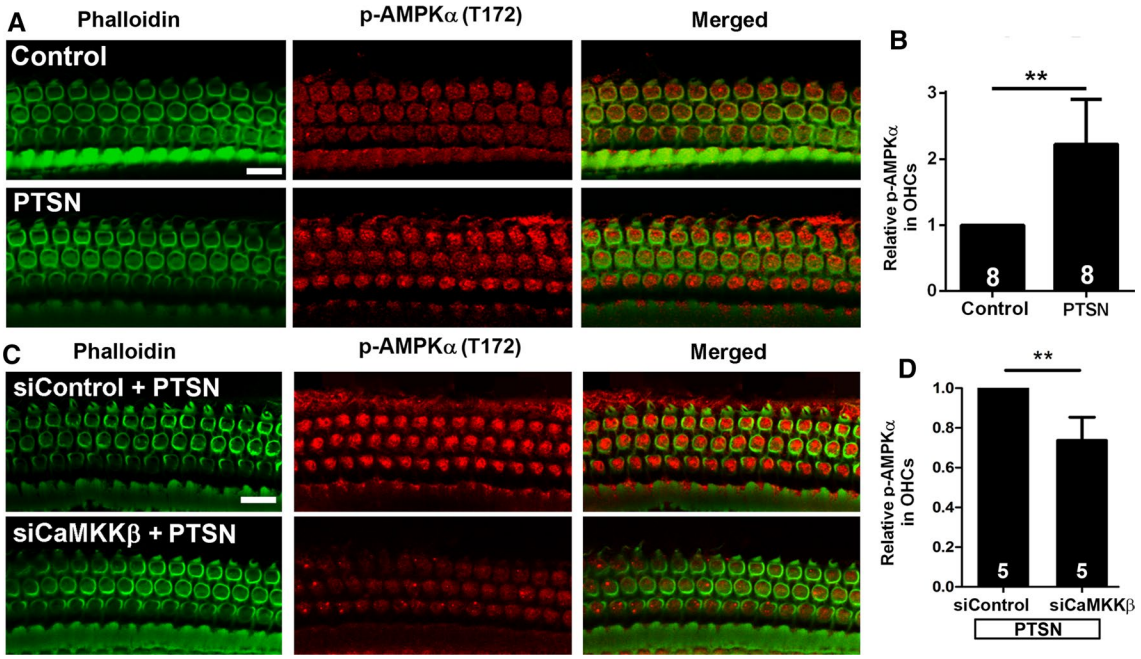

Fig. 10 Silencing CaMKKβ decreases PTS-noise-increased p-AMPKα in OHCs of CBA/J mice. **A** Representative images show that PTSN exposure increases p-AMPKα (T172) in OHCs assessed 1–3 h after the exposure. **B** Semi-quantification of p-AMPKα (T172) in OHCs of the basal turn confirms a significant increase by exposure to PTSN. **C** Representative images show that the PTSN-induced increase in p-AMPKα (T172) immunolabeling (red) is reduced by siCaMKKβ compared to those of siControl mice examined 1–3 h after the exposure. **D** Semi-quantification of p-AMPKα (T172) in the basal turn confirms a significant decrease in siCaMKKβ-treated cochleae. All representative images are from the basal turn, corresponding to sensitivities to 30–32 kHz. Green: phalloidin-stained OHCs. Scale bar = 10 μm. Data for all bar graphs are presented as means + SD, and analyzed by one-sample *t* tests (**B**, **D**, and **F**). The number of animals in each group is indicated in the bar graph, $**p < 0.01$

kinases upstream of AMPKα and is partially responsible for noise-induced AMPKα activation in OHCs.

Discussion

The salient findings of this study are that silencing CaMKKβ via AAV transduction or pretreatment with siCaMKKβ via intra-tympanic delivery significantly attenuates noise-induced hair cell loss and NIHL. The functional and morphological evidence supports that traumatic noise exposure activates CaMKKβ in OHCs, causing changes in pathological signaling related to activation of the CaMKKβ cascade, for example the CaMKKβ–AMPKα pathway. Additionally, this study employed FISH in adult mouse whole-mounts and shRNA via AAV2.7m8 transduction *in-vivo* for investigation of noise-induced hearing loss, proving the feasibility for employing these cutting-edge technologies in adult mice for studying the mechanisms of NIHL.

Exposure to traumatic noise activates CaMKKβ, while inhibition of CaMKKβ by RNA silencing protects from noise-induced hair cell loss and hearing loss in mice

The results that p-CaMKI-positive OHCs appear in the hook and lower basal turn 1–3 h after the exposure agree with the notion that OHCs in the hook and basal turn are more sensitive to noise trauma than those of the apical and middle turns. Protein phosphorylation of CaMKI, acting as one of the markers for CaMKKβ activation, has been well documented [36, 39]. Our data show that p-CaMKI is detected only in the stereocilia and cuticular plates of structurally damaged OHCs, consistent with the notion that calcium overload in OHCs is responsible for the apoptotic and necrotic OHC death observed at earlier time points after inner ear insults [7, 74]. This also aligns with the finding that OHC death is observed initially in the lower basal region and follows a base-to-apex gradient [7, 65, 74] and with literature, showing that calcium overload occurs in OHCs undergoing or very near cell death [12, 13]. Supporting cells and IHCs, which do not undergo cell death after noise exposure conditions that we used, do not display immunolabeling for p-CaMKI. Moreover, the appearance of p-CaMKI (T177) in stereocilia and cuticular plates of OHCs after traumatic exposure is compatible with the notion that CaMKKβ is activated by free calcium entering cochlear OHCs via the mechanoelectrical transducer (MET) channel [16]. However, CaMKKβ mRNA increased significantly in OHCs of the apical, middle, and basal turns 24 h after the exposure, indicating newly synthesized mRNA for a cellular feedback response, while immunolabeling for CaMKKβ increased significantly in OHCs at the basal turn, but not in parallel with mRNA expression in the apical and middle turns, perhaps due to increased protein degradation. The immunolabeling for CaMKKβ was uniformly increased in basal turn OHCs. In this case, we would expect all cells that show immunolabeling for CaMKKβ to eventually complete this pathway and die. The mosaic pattern of p-CaMKI is an asynchronous response of various OHCs to the noise stimulation, where some cells may still remain intact, while others have begun or completed their response to the insults. The immunolabeling for p-CaMKI localizes at the stereocilia and cuticular plates of structurally damaged OHCs, perhaps also associated with noise-induced intracellular calcium release, as associated mitochondria and endoplasmic reticulum (ER) membranes known as Hensen's body conspicuously concentrates in a band beneath the cuticular plate, which acts as large-capacity calcium store [5] with a pathologic release due to calcium overload and purinergic receptor or IP_3 signaling [35, 55]. Additionally, the plasma membrane calcium ATPase (PMCA), the primary mechanism by which calcium is extruded from hair cells, is localized densely in the OHC stereocilia region [11]. The sum of these findings provides an explanation for the positive p-CaMKI specifically at the stereocilia and cuticular plates of OHCs after traumatic noise exposure.

Our functional and morphological evidence using shCaMKKβ via AAV transduction or silencing with siCaMKKβ *in-vivo* further supports that CaMKKβ is the key target for prevention of noise-induced OHC death and hearing loss. Furthermore, activation of CaMKKβ is involved in both noise-induced pathologies of losses of IHC synapses and OHCs; however, there are differences in the degree of protection between OHCs and IHC synapses. For example, inhibition of CaMKKβ by 40% in OHCs via RWM delivery reduces noise-induced OHC loss, while noise-induced loss of synapses is nearly completely prevented. Such a difference in the protection of OHCs and IHC synapses indicates that complete prevention of OHC loss is more difficult to achieve than protection of IHC synapses under the current experimental conditions in CBA/J mice. Our current study exposes CBA/J mice to broadband noise of 2–20 kHz inducing losses of OHCs and IHC synapses at higher frequencies but not at the lower frequencies (6, 8, and 16 kHz), in agreement with our previous report [22]. The deficits of auditory functional measurements, such as elevated auditory brainstem response thresholds at the 16-kHz frequency and diminished DPOAE amplitudes at lower frequencies, may be associated with other pathologies. For example, noise can cause stereocilia injury without loss of the sensory hair cells, affecting their function [21]. Additionally, morphologically intact but physiologically compromised OHCs may also contribute to such a discrepancy as evidenced by OHC functional measurements with DPOAEs. Traumatic

noise exposure causes the DPOAE amplitudes to drop from around + 20 dB SPL to below 0 from 8–36 kHz, while such decreased DPOAE amplitudes are significantly elevated by shCaMKKβ treatment via AAV transduction or pretreatment with siCaMKKβ, indicating preservation of OHC function. Our hypothesis is that the early phase of p-CaMKI expression is triggered by CaMKKβ activation; thus, inhibition of CaMKKβ through shRNA or siRNA before noise exposure can significantly prevent noise-induced hair cell death and hearing loss. This finding does not rule out the participation of other potential mechanisms in NIHL, such as oxidative stress. The over-production of reactive oxygen species (ROS) in the inner ear has emerged as a common mechanism for many traumatic insults, including noise exposure. There is good evidence that ROS are formed in the inner ear following intense sound exposures, specifically in the stria vascularis and the organ of Corti [20, 21, 70, 71]. Indirect indicators of ROS formation have been detected at the onset of the noise exposure and may persist for hours or even days following the exposure. Attesting to the importance of endogenous antioxidants, decreased glutathione in the inner ear enhances noise trauma, while dietary supplementation with glutathione or administration of other antioxidants attenuates NIHL [15, 41]. Our earlier publication also showed that treatment with N-acetylcysteine (NAC) protects against temporary hearing loss in mice [73], in agreement with clinical studies [30, 34]. However, the protective effect against noise-induced permanent hair cell loss by NAC is weaker than that achieved by pretreatment with the AMPKα inhibitor compound C or by silencing AMPKα in CBA/J mice [22, 73], in line with failures of clinical trials [29, 33]. Additionally, we observe over-production of ROS markers in OHCs, such as 4-hydroxynonenal (4-HNE) and 3-nitrotyrosine (3-NT), and markers of transient cellular energy depletion, like p-AMPKα, appear after noise exposure [20, 22, 73]. Recently, we reported that noise-induced over-production of ROS enhances p-AMPKα [68].

Cellular responses in temporary threshold shift (TTS) and PTS insults might overlap; however, activation of CaMKKβ appears only after exposure to traumatic noise causing hair cell loss, not after exposure to lower intensity noise that induces only temporary hearing loss. This clearly suggests that the pathology and mechanisms of NIHL vary with severity of exposure. TTS noise exposure may preferentially activate inner ear endogenous protective systems, such as autophagy [73] and intrinsic cellular survival pathways, such as the antioxidant defense system [48]. Treatment with the autophagy inducer rapamycin attenuates TTS, but the protective effect against noise-induced permanent hair cell loss by rapamycin is minimal [73]. We regard PTS-noise exposure as a condition wherein the trauma has exceeded the endogenous protective system. Additionally, we should caution using TTS as a paradigm for protection since TTS exposure can cause cochlear synaptopathy (also called hidden hearing loss) that manifests late in age [31].

Additionally, we should mention that although a significant difference in the expression of p-CaMKI and CaMKKβ was detected by immunolabeling in OHCs in the hook and lower basal turn, the protein expression levels by Western blotting were equivalent between control samples and experimental samples. We must caution, however, that Western blots were assessed in whole cochlear homogenates due to the limited amount of cochlear tissues in mice. Therefore, changes in the cochlear sensory hair cells in the basal turn might be muted by the overabundance of other cochlear cell types resulting in findings of unchanged protein expression [22, 64].

Finally, although our results utilizing CaMKKβ silencing support the concept that CaMKKβ is one of the kinases upstream of AMPKα in the inner ear, aside from inducing activation of AMPKα, studies from other systems suggest that activated CaMKKβ could also cause accumulation of cytokines, playing a role in regulation of the immune-suppressive microenvironment [39, 46, 47]. Therefore, further studies on activation of CaMKKβ pathways in NIHL are needed to address the details of the molecular and cellular mechanisms of NIHL.

RNAi-based treatment has therapeutic potential for protection from inner ear trauma-induced hearing loss

The target specificity provided by RNA interference makes it a promising tool for medical applications as a bio-therapy. Local application of siRNA is feasible as various surgical approaches for inner ear therapy are used clinically [2]. In recent years, several AAV vectors have been reported to transfect sensory hair cells, and have been used to treat genetic hearing loss [2, 25, 32], providing an ideal tool to mediate gene silencing for the prevention or management of NIHL. Our results support this notion, demonstrating that transduction of shCaMKKβ by AAV vectors protects against NIHL. Since the size of shRNAs are typically about 80 base pairs, the intrinsic limitation of AAV for the small packaging capacity (about 4.5 kb) is not an issue [10, 56]. Our results show that the infection rate of AAV2.7m8 vectors in sensory hair cells of FVB/NJ mice is very high, with a rate of 100% in IHCs and 90% in OHCs in the basal and middle turns, and a lower rate of 40% in the apical turn, in agreement with a previous report [25]. This pattern is appropriate for study of acquired hearing loss induced by inner ear damage in which loss of OHCs follows a base-to-apex gradient. Consistent with the previous publications, injection of

AAV2.7m8 to FVB/NJ p1–2 pups via the cochlear scala media does not affect auditory thresholds [25, 32, 66, 72]. Furthermore, we found that AAV2.7m8 transfection alone or transduction of shControl does not alter OHC sensitivity to traumatic noise exposure.

In this study, we selected FVB/NJ mice for shCaMKKβ AAV transduction, since FVB/NJ mice show normal baseline hearing up to at least 10 weeks of age. Our results show that FVB/NJ mice have similar sensitivity to noise-induced loss of OHCs in the basal turn to that of CBA/J mice, in agreement with the previous report [23]. In general, the AAV infection rate is higher in pups than adults. FVB/NJ mouse breeders are prolific, and mothers continue to take care of their AAV-injected pups. Moreover, we do not see ototoxicity induced by eGFP up to 8 weeks after virus injection to FVB/NJ p1–2 pups. Our data support utilization of FVB/NJ mice for AAV delivery to mediate gene expression for the study of NIHL *in-vivo*. Furthermore, we have not detected any side effects of siCaMKKβ at the doses that we used (0.3 or 0.6 μg/mouse) via intra-tympanic delivery in CBA/J mice. Both CBA/J and FVB/NJ mice show normal baseline hearing after treatment with siCaMKKβ or with shCaMKKβ and maintain good general health without differences in fur appearance or body weight compared to control naive mice. Our previous publication showed that fluorescence-conjugated siRNA was detected in the inner ear 24–48 h after intra-tympanic delivery [43]. The effect most often will last from 5 to 7 days (https://www.sigmaaldrich.com/US/en/technical-documents/technical-article/genomics/gene-expression-and-silencing/sirna-faq). Another study reported that GFP fluorescence was reduced to less than one-tenth of the initial levels 4–7 days after siRNA was introduced into postmitotic neurons [57]. Since siRNA is quickly degraded, long-term adverse effects of siRNA may be inconsequential. ShRNA is transduced via AAV. As viral vectors, AAVs offer an excellent platform for gene therapy due to their safety profile, persistent gene expression in non-dividing cells, target-cell specificity, lack of pathogenicity, and low immunogenicity [2, 3, 9]. Our study suggests that shRNA will provide a powerful tool for investigation of the mechanisms of NIHL.

In summary, our studies highlight a pathological consequence of the activation of CaMKKβ in OHCs in response to traumatic noise exposure. The significant attenuation of noise-induced functional deficits and morphological loss of IHC synapses and OHCs either by shCaMKKβ via AAV transduction or by delivery of naked siCaMKKβ suggest that CaMKKβ is a critical factor contributing to NIHL. This finding should inspire future directions for development of compounds for prevention of NIHL.

Materials and methods

Animals

Male CBA/J mice (stock #00,656) at the age of 10 weeks and FVB/NJ breeder mice (stock #001,800) at the age of 4 weeks were purchased from the Jackson Laboratory. All mice had free access to water and a regular mouse diet (Irradiated Lab Diet #5V75), and were housed in a specific pathogen-free animal facility at MUSC under a standard 12:12 h light–dark cycle with the room kept at 22 ± 1 °C and the background environmental sound levels maintained around 50 dB SPL. FVB/NJ mice were bred in a MUSC animal facility. CBA/J mice had 1 week of acclimation before baseline auditory brainstem response (ABR) measurements. Baseline ABRs of all mice were measured 3–4 d prior to noise exposure. If the baseline auditory thresholds were above 30 dB SPL, mice were excluded from the study. All research protocols were approved by the Institutional Animal Care & Use Committee at MUSC. Animal care was under the supervision of the Division of Laboratory Animal Resources at MUSC.

The sensitivity to NIHL is influenced by a variety of factors, such as age, sex, strain, genetic background, animal care with or without use of dietary enrichments, levels of ambient noise, and circadian rhythms (timing of noise exposure) [51, 63]. All of these factors are well controlled in our experiments and data analysis. We have used both male and female FVB/NJ mice at the age of 4 weeks for assessment of noise-induced hearing loss. Our data show no difference in sensitivity to noise exposure between male and female FVB/NJ mice at the age of 4 weeks when levels of estrogen (a modulating factor of NIHL) are still low in female mice [53]. To eliminate age as another co-founding factor in NIHL, we only used male CBA/J mice at the age of 12 weeks in our experiments.

Measurements of auditory brainstem responses and distortion product otoacoustic emissions

Auditory brainstem response (ABR) measurements were performed 4–5 d before noise exposure and 14 d after the exposure. Briefly, mice were anesthetized with an intraperitoneal (IP) injection of a mixture of xylazine (10 mg/kg) and ketamine (100 mg/kg), and then placed in a soundproof and electrically shielded booth (Acoustic Systems, Austin, TX). Mouse body temperature was maintained near 37 °C with a heating pad. Acoustic stimuli were delivered monaurally to a Beyer earphone attached to a customized plastic speculum inserted into the ear canal. Electrodes were inserted into subcutaneous tissue at the

vertex of the skull and the mastoid regions under the left ear and right ear (ground). ABRs were measured at 8, 16, and 32 kHz. Tucker Davis Technology (TDT) System III hardware and SigGen/Biosig software were used to present the stimuli (15 ms duration tone bursts with 1 ms rise-fall time) and record the response. Up to 1024 responses were averaged for each stimulus level. Thresholds were determined for each frequency by reducing the intensity in 10-dB increments until no organized response was detected. Thresholds were estimated between the lowest stimulus level where a response was observed and the highest level without response. ABR wave II was used to determine thresholds for each frequency and thresholds were assigned by an expert who was blinded to the treatment conditions. DPOAE testing was performed following ABR measurements. The emissions were measured using TDT RZ6 System and SigGen software. The acoustic assembly containing an ER-10B + microphone connected to two transducers was tightly apposed into the ear canal. Primary tones were presented at fixed intensity levels of L1 = 65 dB SPL and L2 = 55 dB SPL with f2/f1 ratio of 1.2. Physiological responses of each mouse were analyzed for individual frequencies and averaged for each of these frequencies from 4 to 36 kHz.

Noise exposure

In this study, male CBA/J mice at the age of 12 weeks and both sexes of FVB/NJ at 4 weeks were exposed to broadband noise (BBN) with a frequency spectrum from 2 to 20 kHz; exposure of male CBA/J mice at 101 dB sound pressure level (SPL) for 2 h inducing loss of IHC synaptic ribbons, loss of OHCs, and permanent threshold shifts (PTS) 14 d after the noise exposure. These are referred to as our PTS-noise conditions (PTSN). FVB/NJ mice were exposed to 100 dB SPL inducing PTS. Generally, four unrestrained mice were exposed in the morning in the sound chamber for 2 h with one mouse per stainless steel wire cage (approximately 9 cm^3). Sound levels of the noise exposure were measured with a sound level meter at multiple locations within the sound chamber to ensure uniformity of the sound field, and were measured before and after exposure to ensure stability. The sound exposure chamber was fitted with a loudspeaker (model 2450H; JBL) driven by a power amplifier (model XLS 202D; Crown Audio) fed from a CD player (model CD-200; Tascam TEAC American). Audio CD sound files were created and equalized with audio editing software (Audition 3; Adobe Systems, Inc.). The background sound intensity of the environment surrounding the cages was 65 dB as measured with a sound level meter (model 1200; Quest Technologies). Control mice were kept in silence (without use of the loudspeaker) in the cages within the same chamber for 2 h.

Delivery of an AAV vector into the inner ear of FVB/NJ pups on postnatal day 1–2

AAV2.7m8 capsid plasmids, backbone vector plasmids, and helper plasmids were purchased from Addgene (#64,839, #85,451, and #112,867). Sequences of control and CaMKKβ shRNA were obtained from Sigma-Aldrich (Control: 5′-CCGGG CGC GAT AGC GCT AAT TTC TCG AGA AAT TAT TAG CGC TAT CGC GC TTTTTG-3′, CaMKKβ: 5′-CCGGG TAT CCA CTT GGG CAT GGA ATC TCG AGA TTC CAT GCC CAA GTG GAT AC TTTTTG-3′) and reconstructed into vector plasmids by Synbio Technologies. Final AAV production was performed by the vector core of the University of Pennsylvania at titer 2.5×10^{13} GC/mL and stored at—80 °C before use. The schematic of the AAV vector plasmid and the experimental protocol is illustrated in Fig. 3D. Briefly, FVB/NJ pups (p1–2) were injected into the RWM using beveled glass microinjection pipettes. Pipettes were pulled from capillary glass (WPI, Sarasota, FL) on a P-2000 pipette puller (Sutter Instrument, Novato, CA). The tip was cut roughly a 30° angle. Pups were anesthetized by rapid induction of hypothermia in ice/water for 2 min until loss of consciousness, and then placed on cooling platform for about 10 min during the surgery. The surgical site (left ear area) was disinfected by wiping with 70% ethanol. A 0.6-cm retroauricular incision behind the left ear was made to expose the transparent otic bulla and the glass micropipette tip was advanced manually through the bulla, overlying fascia, and the RWM. Approximately 2 µL of virus at the above concentration was injected over 5 min (Nanoliter injector controlled by MICRO4 controller, World Precision Instruments). The skin incision is closed with 5–0 nylon sutures. The pups were allowed to recover from anesthesia on warmed pad (about 37 °C) for about 5 min and then returned back to their mothers to be nursed until weaning. A schematic diagram indicated experimental timeline (Fig. 1F).

Intra-tympanic delivery of siRNA 72 h before noise exposure to CBA/J mice

siCaMKKβ (Invitrogen, #n437808) or scrambled RNA control (siControl, Invitrogen, #4,390,843) was delivered locally via intra-tympanic application onto RWN as previously described [43] Briefly, after anesthesia, the left ear post-auricular region was shaved and disinfected with 10% povidone-iodine. Under the operating microscope, a retroauricular incision (about 1.0 cm) was made to approach the temporal bone. The otic bulla was identified ventral to the facial nerve and a shallow hole was made in the thin part of the otic bulla with a 30-G needle and enlarged to a diameter of 2 mm to visualize the RWN. Customized sterile micro-medical tubing was inserted into the hole just above

the RWN to slowly deliver 10 µL (0.6 µg or 0.3 µg per ear) of pre-designed siCaMKKβ or siControl. After the siRNA was delivered, the hole in the otic bulla was covered with surrounding muscle and glued with tissue adhesive (3 M Vetbond Tissue Adhesive). Finally, the skin incision was closed with tissue adhesive and the mouse was kept in the surgical position during recovery from anesthesia (about 1 h). Seventy-two hours after siRNA delivery, the animals were exposed to PTSN.

Myosin VIIa labeling and DAB staining of cochlear whole-mount surface preparations for hair cell counts

The auditory sensory hair cells are located on the basilar membrane, organized in a tonotopic fashion with high-frequency detection occurring in the base and low frequency in the apex. Whole-mount surface preparations allow us to distinguish the regions of the cochlea and the effects of treatments on sensory hair cells in these different regions. The procedures for whole-mount surface preparations and diaminobenzidine (DAB) staining of cochlear epithelia were followed as previously described [7, 14]. Briefly, the temporal bones were removed immediately following decapitation and slowly perfused through the round and oval windows with a solution of 4% paraformaldehyde in phosphate-buffered saline, pH 7.4 (PBS) and kept in this fixative overnight at 4 °C. Between every step, the cochlear samples were washed at least three times with PBS for 5–10 min each wash. After decalcification with 4% sodium EDTA solution (adjusted with HCl to pH 7.4) for 2–3 d at 4 °C, the cochleae were micro-dissected into apical, middle, and basal segments and adhered to 10-mm round coverslips (Microscopy Products for Science and Industry, #260,367) with cell-Tak (Corning, #354,240). The specimens were first permeabilized in 2% Triton X-100 (Sigma-Aldrich, #T9284) and then blocked with 10% goat serum (GS) each for 30 min at room temperature (RT), followed by incubation with primary polyclonal rabbit anti-myosin VIIa antibody (Proteus Bioscience, #25–6790) at a 1:200 dilution for 24 h at 4 °C. Next, the specimens were incubated with biotinylated goat anti-rabbit secondary antibody (Vector Laboratories, #BA-1000) at a 1:200 dilution overnight at 4 °C and followed with ABC solution (Vector Laboratories, # PK-4100) overnight and DAB staining buffer for 5 min, as necessary for sufficient staining intensity. Finally, 8 µL of mounting medium (Electron Microscopy Sciences, #17,985-10) was added to the specimens on the round coverslips and covered with another round coverslip on microscope slides, the two slips sandwiched together and sealed with nail polish. Images were taken with Zeiss AxioCam MRc5 camera with Axioplan 2 imaging software with a Zeiss microscopes.

Images from the apex through the base of the DAB-stained surface preparations were captured using the 20× magnification lens on the Zeiss microscope. The lengths of the cochlear epithelia were measured and recorded in millimeters. Since there was no or very mild inner hair cell (IHC) loss in our PTS-noise condition, only OHCs were counted from the apex to the base along the entire length of the mouse cochlear spiral. Percentages of OHC loss in each 0.25- or 0.5-mm length of epithelium were plotted as a function of the cochlear length as a cytocochleogram [7].

Based on the previous literature [38, 60], mapping of frequencies as a function of distance along the entire length of the cochlear spiral and distinction between cochlear apical, middle, basal, and hook turns was illustrated in a schematic diagram (Fig. 1E).

Immunocytochemistry for cochlear whole-mount surface preparations

The surface preparation and sample mounting techniques were identical to those described in the above section "Myosin VIIa labeling and DAB staining of cochlear epithelia". After blocking with 10% goat serum, the specimens were incubated with primary antibodies: polyclonal rabbit anti-CaMKKβ at 1:200 (Invitrogen, #PA5-82,589), polyclonal rabbit anti-p-CaMKI (Thr 177) at 1:50 (Invitrogen, #PA5-38,434), and monoclonal rabbit anti-p-AMPKα (Thr 172) at 1:200 (Cell Signaling Technology, # 2535) in darkness at 4 °C for 24 h, and then incubated with the Alexa-Fluor-594-conjugated secondary antibody (Thermofisher Scientific, #A11012) at a concentration of 1:200 at 4 °C overnight and followed with incubation with Alexa-Flour-488-phalloidin (Invitrogen, #A12379) for 1 h at RT in darkness. Secondary antibody controls were routinely processed without incubation with primary antibodies.

For immunolabeling of IHC synapses, the specimens were incubated in darkness at 37 °C overnight with primary monoclonal mouse anti-CtBP2 IgG1 at 1:200 (BD Biosciences, #612,044) and mouse anti-GluA2 IgG2a at 1:2,000 (Millipore, #MAB397), followed by the Alexa-Fluor-594 goat anti-mouse IgG1 and Alexa-Fluor-488 goat anti-mouse IgG2a (1:1,000) at 37 °C for 1 h in darkness.

Immunolabeled images were taken with a 63× magnification lens under identical Z-stack conditions using a Zeiss LSM 880.

Semi-quantification of the immunofluorescence signals from whole-mount surface preparations

Immunohistochemistry has been well accepted as a semi-quantitative methodology when used with careful consideration of the utility and semi-quantitative nature of these assays [58, 61]. We first detected specificity of antibodies

by Western blot analysis. Antibodies showing only a single band with the correct molecular weight were used for immunolabeling on surface preparations and quantification of immunolabeling in OHCs.

Immunofluorescence of CaMKKβ, p-CaMKI (T177), and p-AMPKα (T172) on whole-mount surface preparations was quantified from original confocal images, each taken with a 63 × magnification lens under identical conditions and equal parameter settings for laser gains and PMT gains, using the ImageJ software (National Institutes of Health, Bethesda, MD). The cochleae from the different groups were fixed and stained simultaneously with identical solutions and processed in parallel. All of the surface preparations were counter-stained with Alexa Fluor 488 phalloidin (green) to label hair cell structure to identify the comparable parts of the hair cells in confocal images. The regions of interest of individual OHCs were outlined with the circle tool based on phalloidin staining. The grayscale values were determined in the OHCs to quantify the changes in fluorescence intensity. The immunolabeling for the target proteins in cochlear OHCs were measured in the apical (around 1 mm from the apex; corresponding to sensitivity to 8 kHz), middle (around 2.4 mm from the apex; corresponding to sensitivity to 16 kHz), and basal turns (around 3.9 mm from the apex; corresponding to sensitivity to 32 kHz) of cochlear epithelia in 0.12-mm segments, each containing about 60 OHCs. The intensity of the background was subtracted and average grayscale intensity per cell was then calculated. For each repetition, the relative grayscale value was determined by normalizing the ratio to control.

The pathology of NIHL varies with severity of exposure. OHCs are more sensitive than IHCs. The noise conditions that we selected can induce OHC loss, but not IHC loss. Furthermore, we only observed p-CaMKI in OHCs (and not in IHCs) in the basal and hook turns. We, therefore, have focused on OHCs in this study and performed semi-quantification of the immunolabeling for CaMKKβ and p-AMPKα in OHCs in the basal turn. The schematic diagram of OHCs (Fig. 1D) indicated the plane from which confocal immunofluorescence were captured for quantification, the cytosolic area between the two red lines.

Whole-mount fluorescent in-situ hybridization with RNAscope

The RNAscope multiplex fluorescent reagent kit v2 (cat #323,100) and the CaMKKβ probe (cat #529,851) were purchased from ACD. The procedures for FISH with RNAscope were performed in RNase-free conditions and followed as per the manufacturer's instructions and as previously described [27, 49]. Each step was followed with washing with RNase-free wash buffer three times at RT for 5 min each wash. All solutions were pretreated with 0.1% diethyl pyrocarbonate (DEPC, Sigma, #D5758). After fixation (4% PFA for 24 h) and decalcification (0.6% EDTA for 7 d), the cochlear epithelia were dissected into apex, middle, and basal turns as described above for surface preparations. Specimens were dehydrated in a graded ethanol (EtOH) series (50%, 70%, and 100%) with gentle agitation at RT for 5 min each. RNA retrieval was performed at 99 °C for 20 min in retrieval buffer (ACD, #323,110) and then incubated with protease III (ACD, #323,110) at 40 °C for 30 min, followed with 0.05% Tween 20 at RT for 30 min. The specimens were incubated with CaMKKβ probe solution at 40 °C overnight and amplified with three pre-amplifier hybridization solutions (Amp1, 2, and 3) one-by-one at 40 °C for 30 min for Amp1 and Amp2, and 15 min for Amp3. The specimens were then incubated with Opal-620 (Akoya Bioscience) for 30 min at 40 °C, followed with an immunolabeling protocol using rabbit polyclonal anti-myosin VIIa primary antibody (Proteus Bioscience, #25–6790, 1:200) and Alexa-Fluor-488-conjugated secondary antibody (Thermofisher Scientific, #A11094, 1:200) at 4 °C overnight. Finally, the specimens were incubated with Opal-620 again and 4',6-diamidino-2-phenylindole (DAPI, Thermo Fisher Scientific, #62,247) for 10 min at RT. The specimens were mounted as described above.

Quantification of the immunolabeled ribbons or RNAscope puncta from Z projections on whole-mount surface preparations

We have followed a procedure as previously described [22]. The number of presynaptic ribbons labeled with CtBP2 or probed with CaMKKβ on surface preparations was quantified from original confocal images, each taken with a 63 × magnification lens under identical Z-stack conditions (in 0.25-µm Z-steps) and equal parameter settings for laser gains and PMT gains. The Z-stack images in each 0.12-mm segment (containing about 16 IHCs) were captured from cochlear surface preparations. The number of synaptic ribbons or CaMKKβ mRNA puncta was counted using ImageJ software (National Institutes of Health, Bethesda, MD). Briefly, the background of the images was subtracted, the noise was despeckled once, and the threshold was set to isolate the immunolabeling of ribbons or the CaMKKβ mRNA puncta signals. The image was then converted to a binary file and the number of ribbon particles or CaMKKβ mRNA puncta was counted using the 3D Object Counter. The number of synaptic ribbons or CaMKKβ mRNA puncta was divided by the total number of IHCs or OHC nuclei within the image. For each set of experiments, the cochleae from both control and PTS-noise groups were fixed and stained simultaneously with identical solutions and processed in parallel.

Extraction of total protein from mouse cochleae

Cochleae were rapidly removed and dissected in ice-cold PBS, pH 7.4, containing Complete Mini EDTA-free protease inhibitor cocktail tablets (Sigma-Aldrich, #11,836,170,001). To extract total protein from mouse cochleae, tissues from the cochleae of a single mouse were homogenized in ice-cold RIPA lysis buffer (Sigma-Aldrich, #R0278) with the cocktail proteinase inhibitors plus phosphatase inhibitor cocktails II and III (Sigma-Aldrich, #P5726 and #P0044) using a glass/glass micro-tissue grind pestle and vessel for 5 min. Tissue debris were removed by centrifugation at $10,000 \times g$ at 4 °C for 10 min and the supernatants were retained as the total protein fractions. Protein concentrations were determined using the Bio-Rad Protein Assay dye reagent (Bio-Rad, #500-0114) with bovine serum albumin as a protein standard. Two ears from each mouse were collected for each sample and stored at -80 °C.

Western blot analysis

Protein samples (30 µg) from mouse cochlear homogenates were separated by SDS-PAGE. After electrophoresis, the proteins were transferred onto a PVDF membrane (Bio-rad, #1,620,177) and blocked with 5% albumin from bovine serum (Sigma-Aldrich, #A7906) in PBS-0.1% Tween-20 (PBS-T) (Sigma-Aldrich, #P1379). The membranes were incubated with anti-CaMKKβ (1:1,000, Invitrogen, #PA5-30,399), anti-p-CaMKI (T177) (1:1,000, Invitrogen, #PA5-38,434), or anti-GAPDH (1:5,000, Millipore, #ABS16) at 4 °C overnight, and then washed three times (10 min each) with PBS-T buffer. Membranes were incubated with an appropriate secondary antibody (Cell signaling technology, #7074 or #7076) at a concentration of 1:3,000 for 1 h at RT. Following extensive washing of the membrane, the immunoreactive bands were visualized by SuperSignal West Dura Extended Duration (Thermo Scientific, #34,075).

Western blot bands were scanned by LI-COR Odyssey Fc imaging system and analyzed using Image J software. First, the background staining density for each band was subtracted from the band density. Next, the probing protein/GAPDH ratio was calculated from the band densities run on the same gel to normalize for differences in protein loading. Finally, the difference in the ratio of the control and experimental bands was tested for statistical significance.

Statistical analysis

Data were analyzed using SYSTAT 8.0 and GraphPad 5.0 software for Windows. Biological sample sizes were determined based on the variability of measurements and the magnitude of the differences between groups, as well as experience from our previous studies, with stringent assessments of difference. We have used the *t* test to determine if there is a significant difference between the means of two groups. Differences for single-pair comparisons were analyzed using two-tailed unpaired Student's *t* tests. Data for relative ratios of single-pair comparisons were analyzed with one-sample *t* tests. To determine whether there are any statistically significant differences between the means of three or more independent groups, we have used one-way analysis of variance (ANOVA). F values have been used in one-way ANOVA and calculated by the variation between sample means divided by variation within the samples. To determine which specific groups are different from each other, post hoc tests were followed ANOVA calculations. A p value < 0.05 was considered statistically significant. Data are presented as individual mice and means + or ± SD based on the sample size and variability within groups. Sample sizes are indicated for each figure.

Supplementary Information The online version contains supplementary material available at https://doi.org/10.1007/s00018-022-04268-4.

Acknowledgements We thank Dr. Jochen Schacht for his valuable comments on the manuscript. We also thank Dr. Yuan Shao in the MUSC Biorepository & Tissue Analysis Shared Resource for technical assistance with *in-situ* hybridization RNAscope and Andra Talaska for proofreading of the manuscript.

Author contributions FW, KH, QF authors have contributed equally to this work. SS designed research; FW, KH, QF, ZH, HZ, XW, and HX performed research; FW, KH, QF, and SS analyzed data; FW, KH, and SS wrote the paper. All authors have reviewed the contents of the manuscript, approve of its contents, and validate the accuracy of the data.

Funding The research project described was supported by grant R01 DC009222 from the National Institute on Deafness and Other Communication Disorders, National Institutes of Health. All experiments described in this manuscript were conducted in the WR Building at Medical University of South Carolina in renovated space supported by grant C06 RR014516. Animals were housed in MUSC CRI animal facilities supported by grant C06 RR015455 from the Extramural Research Facilities Program of the National Center for Research Resources.

Availability of data and materials All data generated or analyzed during this study are included in this published article and its supplementary information files.

Declarations

Conflict of interests The authors declare that they have no competing interests.

Ethics approval and consent to participate No human data or tissue were involved. All animal research protocols were approved by the Institutional Animal Care & Use Committee at MUSC. Animal care was under the supervision of the Division of Laboratory Animal Resources at MUSC.

Consent for publication Not applicable.

References

1. Anderson KA, Ribar TJ, Lin F, Noeldner PK, Green MF, Muehlbauer MJ, Witters LA, Kemp BE, Means AR (2008) Hypothalamic CaMKK2 contributes to the regulation of energy balance. Cell Metab 7:377–388
2. Askew C, Chien WW (2020) Adeno-associated virus gene replacement for recessive inner ear dysfunction: Progress and challenges. Hear Res 394:107947
3. Bankoti K, Generotti C, Hwa T, Wang L, O'Malley BW Jr, Li D (2021) Advances and challenges in adeno-associated viral inner-ear gene therapy for sensorineural hearing loss. Molecular therapy Methods & clinical development 21:209–236
4. Carling D (2017) AMPK signalling in health and disease. Curr Opin Cell Biol 45:31–37
5. Ceriani F, Mammano F (2012) Calcium signaling in the cochlea - Molecular mechanisms and physiopathological implications. Cell Commun Signal 10:20
6. Chakraborty C, Sharma AR, Sharma G, Doss CGP, Lee SS (2017) Therapeutic miRNA and siRNA: moving from bench to clinic as next generation medicine. Mol Ther Nucleic Acids 8:132–143
7. Chen FQ, Zheng HW, Hill K, Sha SH (2012) Traumatic noise activates rho-family GTPases through transient cellular energy depletion. J Neurosci 32:12421–12430
8. Chen J, Hill K, Sha SH (2016) Inhibitors of histone deacetylases attenuate noise-induced hearing loss. J Assoc Res Otolaryngol 17:289–302
9. Crane R, Conley SM, Al-Ubaidi MR, Naash MI (2021) Gene therapy to the retina and the cochlea. Front Neurosci 15:652215
10. Dong JY, Fan PD, Frizzell RA (1996) Quantitative analysis of the packaging capacity of recombinant adeno-associated virus. Hum Gene Ther 7:2101–2112
11. Dumont RA, Lins U, Filoteo AG, Penniston JT, Kachar B, Gillespie PG (2001) Plasma membrane Ca2+-ATPase isoform 2a is the PMCA of hair bundles. J Neurosci 21:5066–5078
12. Esterberg R, Hailey DW, Coffin AB, Raible DW, Rubel EW (2013) Disruption of intracellular calcium regulation is integral to aminoglycoside-induced hair cell death. J Neurosci 33:7513–7525
13. Esterberg R, Hailey DW, Rubel EW, Raible DW (2014) ER-mitochondrial calcium flow underlies vulnerability of mechanosensory hair cells to damage. J Neurosci 34:9703–9719
14. Fang QJ, Wu F, Chai R, Sha SH (2019) Cochlear surface preparation in the adult mouse. J Vis Exp. https://doi.org/10.3791/60299
15. Fetoni AR, Paciello F, Rolesi R, Paludetti G, Troiani D (2019) Targeting dysregulation of redox homeostasis in noise-induced hearing loss: Oxidative stress and ROS signaling. Free Radic Biol Med 135:46–59
16. Fettiplace R (2017) Hair cell transduction, tuning, and synaptic transmission in the mammalian cochlea. Compr Physiol 7:1197–1227
17. Fridberger A, Flock A, Ulfendahl M, Flock B (1998) Acoustic overstimulation increases outer hair cell Ca2+ concentrations and causes dynamic contractions of the hearing organ. Proc Natl Acad Sci U S A 95:7127–7132
18. Grotemeier A, Alers S, Pfisterer SG, Paasch F, Daubrawa M, Dieterle A, Viollet B, Wesselborg S, Proikas-Cezanne T, Stork B (2010) AMPK-independent induction of autophagy by cytosolic Ca2+ increase. Cell Signal 22:914–925
19. Hardie DG (2003) Minireview: the AMP-activated protein kinase cascade: the key sensor of cellular energy status. Endocrinology 144:5179–5183
20. He Z-H, Pan S, Zheng H-W, Fang Q-J, Hill K, Sha S-H (2021) Treatment with calcineurin inhibitor fk506 attenuates noise-induced hearing loss. Front Cell Develop Biol. https://doi.org/10.3389/fcell.2021.648461
21. Henderson D, Bielefeld EC, Harris KC, Hu BH (2006) The role of oxidative stress in noise-induced hearing loss. Ear Hear 27:1–19
22. Hill K, Yuan H, Wang X, Sha SH (2016) Noise-induced loss of hair cells and cochlear synaptopathy are mediated by the activation of AMPK. J Neurosci 36:7497–7510
23. Ho MK, Li X, Wang J, Ohmen JD, Friedman RA (2014) FVB/NJ mice demonstrate a youthful sensitivity to noise-induced hearing loss and provide a useful genetic model for the study of neural hearing loss. Audiol Neurotol Extra 4:1–11
24. Hurley RL, Anderson KA, Franzone JM, Kemp BE, Means AR, Witters LA (2005) The Ca2+/calmodulin-dependent protein kinase kinases are AMP-activated protein kinase kinases. J Biol Chem 280:29060–29066
25. Isgrig K, McDougald DS, Zhu J, Wang HJ, Bennett J, Chien WW (2019) AAV2.7m8 is a powerful viral vector for inner ear gene therapy. Nat Commun 10:427
26. Jeon SM (2016) Regulation and function of AMPK in physiology and diseases. Exp Mol Med 48:e245
27. Kersigo J, Pan N, Lederman JD, Chatterjee S, Abel T, Pavlinkova G, Silos-Santiago I, Fritzsch B (2018) A RNAscope whole mount approach that can be combined with immunofluorescence to quantify differential distribution of mRNA. Cell Tissue Res 374:251–262
28. Kimura Y, Corcoran EE, Eto K, Gengyo-Ando K, Muramatsu MA, Kobayashi R, Freedman JH, Mitani S, Hagiwara M, Means AR, Tokumitsu H (2002) A CaMK cascade activates CRE-mediated transcription in neurons of Caenorhabditis elegans. EMBO Rep 3:962–966
29. Kopke R, Slade MD, Jackson R, Hammill T, Fausti S, Lonsbury-Martin B, Sanderson A, Dreisbach L, Rabinowitz P, Torre P 3rd, Balough B (2015) Efficacy and safety of N-acetylcysteine in prevention of noise induced hearing loss: a randomized clinical trial. Hear Res 323:40–50
30. Kramer S, Dreisbach L, Lockwood J, Baldwin K, Kopke R, Scranton S, O'Leary M (2006) Efficacy of the antioxidant N-acetylcysteine (NAC) in protecting ears exposed to loud music. J Am Acad Audiol 17:265–278
31. Kujawa SG, Liberman MC (2009) Adding insult to injury: cochlear nerve degeneration after "temporary" noise-induced hearing loss. J Neurosci 29:14077–14085
32. Landegger LD, Pan B, Askew C, Wassmer SJ, Gluck SD, Galvin A, Taylor R, Forge A, Stankovic KM, Holt JR, Vandenberghe LH (2017) A synthetic AAV vector enables safe and efficient gene transfer to the mammalian inner ear. Nat Biotechnol 35:280–284
33. Le Prell CG, Hammill TL, Murphy WJ (2019) Noise-induced hearing loss and its prevention: Integration of data from animal models and human clinical trials. J Acoust Soc Am 146:4051
34. Lin CY, Wu JL, Shih TS, Tsai PJ, Sun YM, Ma MC, Guo YL (2010) N-Acetyl-cysteine against noise-induced temporary threshold shift in male workers. Hear Res 269:42–47
35. Mammano F, Frolenkov GI, Lagostena L, Belyantseva IA, Kurc M, Dodane V, Colavita A, Kachar B (1999) ATP-Induced Ca(2+) release in cochlear outer hair cells: localization of an inositol triphosphate-gated Ca(2+) store to the base of the sensory hair bundle. J Neurosci 19:6918–6929
36. Marcelo KL, Means AR, York B (2016) The Ca(2+)/Calmodulin/CaMKK2 Axis: Nature's Metabolic CaMshaft. Trends Endocrinol Metab 27:706–718
37. Means AR (2000) Regulatory cascades involving calmodulin-dependent protein kinases. Mol Endocrinol 14:4–13
38. Muller M, von Hunerbein K, Hoidis S, Smolders JW (2005) A physiological place-frequency map of the cochlea in the CBA/J mouse. Hear Res 202:63–73
39. Najar MA, Rex DAB, Modi PK, Agarwal N, Dagamajalu S, Karthikkeyan G, Vijayakumar M, Chatterjee A, Sankar U, Prasad TSK (2021) A complete map of the Calcium/

calmodulin-dependent protein kinase kinase 2 (CAMKK2) signaling pathway. J Cell Commun Signal 15:283–290
40. Nyberg S, Abbott NJ, Shi X, Steyger PS, Dabdoub A (2019) Delivery of therapeutics to the inner ear: The challenge of the blood-labyrinth barrier. Sci Transl Med. https://doi.org/10.1126/scitranslmed.aao0935
41. Ohinata Y, Yamasoba T, Schacht J, Miller JM (2000) Glutathione limits noise-induced hearing loss. Hear Res 146:28–34
42. Ohlemiller KK (2019) Mouse methods and models for studies in hearing. J Acoust Soc Am 146:3668
43. Oishi N, Chen FQ, Zheng HW, Sha SH (2013) Intra-tympanic delivery of short interfering RNA into the adult mouse cochlea. Hear Res 296:36–41
44. Orrenius S, Zhivotovsky B, Nicotera P (2003) Regulation of cell death: the calcium-apoptosis link. Nat Rev Mol Cell Biol 4:552–565
45. Pfisterer SG, Mauthe M, Codogno P, Proikas-Cezanne T (2011) Ca2+/calmodulin-dependent kinase (CaMK) signaling via CaMKI and AMP-activated protein kinase contributes to the regulation of WIPI-1 at the onset of autophagy. Mol Pharmacol 80:1066–1075
46. Racioppi L, Nelson ER, Huang W, Mukherjee D, Lawrence SA, Lento W, Masci AM, Jiao Y, Park S, York B, Liu Y, Baek AE, Drewry DH, Zuercher WJ, Bertani FR, Businaro L, Geradts J, Hall A, Means AR, Chao N, Chang CY, McDonnell DP (2019) CaMKK2 in myeloid cells is a key regulator of the immune-suppressive microenvironment in breast cancer. Nat Commun 10:2450
47. Racioppi L, Noeldner PK, Lin F, Arvai S, Means AR (2012) Calcium/calmodulin-dependent protein kinase kinase 2 regulates macrophage-mediated inflammatory responses. J Biol Chem 287:11579–11591
48. Ryan AF, Bennett TM, Woolf NK, Axelsson A (1994) Protection from noise-induced hearing loss by prior exposure to a nontraumatic stimulus: role of the middle ear muscles. Hear Res 72:23–28
49. Salehi P, Nelson CN, Chen Y, Lei D, Crish SD, Nelson J, Zuo H, Bao J (2018) Detection of single mRNAs in individual cells of the auditory system. Hear Res 367:88–96
50. Selbert MA, Anderson KA, Huang QH, Goldstein EG, Means AR, Edelman AM (1995) Phosphorylation and activation of Ca(2+)-calmodulin-dependent protein kinase IV by Ca(2+)-calmodulin-dependent protein kinase Ia kinase. Phosphorylation of threonine 196 is essential for activation. J Biol Chem 270:17616–17621
51. Sha SH, Schacht J (2017) Emerging therapeutic interventions against noise-induced hearing loss. Expert Opin Investig Drugs 26:85–96
52. Shende P, Patel C (2019) siRNA: an alternative treatment for diabetes and associated conditions. J Drug Target 27:174–182
53. Shuster B, Casserly R, Lipford E, Olszewski R, Milon B, Viechweg S, Davidson K, Enoch J, McMurray M, Rutherford MA, Ohlemiller KK, Hoa M, Depireux DA, Mong JA, Hertzano R (2021) Estradiol protects against noise-induced hearing loss and modulates auditory physiology in female mice. Int J Mol Sci. https://doi.org/10.3390/ijms222212208
54. Skelding KA, Rostas JA (2012) The role of molecular regulation and targeting in regulating calcium/calmodulin stimulated protein kinases. Adv Exp Med Biol 740:703–730
55. Spicer SS, Thomopoulos GN, Schulte BA (1999) Novel membranous structures in apical and basal compartments of inner hair cells. J Comp Neurol 409:424–437
56. Sun L, Li J, Xiao X (2000) Overcoming adeno-associated virus vector size limitation through viral DNA heterodimerization. Nat Med 6:599–602
57. Tanaka M, Asaoka M, Yanagawa Y, Hirashima N (2011) Long-term gene-silencing effects of siRNA introduced by single-cell electroporation into postmitotic CNS neurons. Neurochem Res 36:1482–1489
58. Taylor CR, Levenson RM (2006) Quantification of immunohistochemistry–issues concerning methods, utility and semiquantitative assessment II. Histopathology 49:411–424
59. Ulfendahl M, Scarfone E, Flock A, Le Calvez S, Conradi P (2000) Perilymphatic fluid compartments and intercellular spaces of the inner ear and the organ of Corti. Neuroimage 12:307–313
60. Viberg A, Canlon B (2004) The guide to plotting a cochleogram. Hear Res 197:1–10
61. Walker RA (2006) Quantification of immunohistochemistry–issues concerning methods, utility and semiquantitative assessment I. Histopathology 49:406–410
62. Wan G, Gomez-Casati ME, Gigliello AR, Liberman MC, Corfas G (2014) Neurotrophin-3 regulates ribbon synapse density in the cochlea and induces synapse regeneration after acoustic trauma. Elife. https://doi.org/10.7554/eLife.03564
63. Wang J, Puel JL (2018) Toward Cochlear Therapies. Physiol Rev 98:2477–2522
64. Wang X, Zhu Y, Long H, Pan S, Xiong H, Fang Q, Hill K, Lai R, Yuan H, Sha SH (2018) Mitochondrial calcium transporters mediate sensitivity to noise-induced losses of hair cells and cochlear synapses. Front Mol Neurosci 11:469
65. Wang Y, Hirose K, Liberman MC (2002) Dynamics of noise-induced cellular injury and repair in the mouse cochlea. J Assoc Res Otolaryngol 3:248–268
66. Wang Y, Sun Y, Chang Q, Ahmad S, Zhou B, Kim Y, Li H, Lin X (2013) Early postnatal virus inoculation into the scala media achieved extensive expression of exogenous green fluorescent protein in the inner ear and preserved auditory brainstem response thresholds. J Gene Med 15:123–133
67. Winder WW, Thomson DM (2007) Cellular energy sensing and signaling by AMP-activated protein kinase. Cell Biochem Biophys 47:332–347
68. Wu F, Xiong H, Sha S (2020) Noise-induced loss of sensory hair cells is mediated by ROS/AMPKalpha pathway. Redox Biol 29:101406
69. Xiong H, Long H, Pan S, Lai R, Wang X, Zhu Y, Hill K, Fang Q, Zheng Y, Sha SH (2019) Inhibition of histone methyltransferase G9a attenuates noise-induced cochlear synaptopathy and hearing loss. J Assoc Res Otolaryngol 20:217–232
70. Yamane H, Nakai Y, Takayama M, Konishi K, Iguchi H, Nakagawa T, Shibata S, Kato A, Sunami K, Kawakatsu C (1995) The emergence of free radicals after acoustic trauma and strial blood flow. Acta Otolaryngol Suppl 519:87–92
71. Yamashita D, Jiang HY, Schacht J, Miller JM (2004) Delayed production of free radicals following noise exposure. Brain Res 1019:201–209
72. Yu Q, Wang Y, Chang Q, Wang J, Gong S, Li H, Lin X (2014) Virally expressed connexin26 restores gap junction function in the cochlea of conditional Gjb2 knockout mice. Gene Ther 21:71–80
73. Yuan H, Wang X, Hill K, Chen J, Lemasters J, Yang SM, Sha SH (2015) Autophagy attenuates noise-induced hearing loss by reducing oxidative stress. Antioxid Redox Signal 22:1308–1324
74. Zheng HW, Chen J, Sha SH (2014) Receptor-interacting protein kinases modulate noise-induced sensory hair cell death. Cell Death Dis 5:e1262